Coordination Chemistry Reviews, 38 (1981) 89–138
Elsevier Scientific Publishing Company, Amsterdam—Printed in The Netherlands

ELECTRONIC STRUCTURES OF TRANSITION METAL CLUSTER COMPLEXES

MARK C. MANNING and WILLIAM C. TROGLER

Department of Chemistry, Northwestern University, Evanston, Illinois 60201 (U.S.A.)

(Received 22 January 1981)

CONTENTS

A. Introduction 89
B. Theoretical background 91
(i) Techniques 92
(ii) Naked atom clusters 95
(iii) Trinuclear cluster complexes 100
(iv) Tetranuclear cluster complexes 107
(v) Pentanuclear cluster complexes 110
(vi) Hexanuclear cluster complexes 111
(vii) Higher nuclearity cluster complexes 113
C. Spectroscopic studies 113
(i) Photoelectron spectroscopy 113
(ii) Optical spectroscopy 115
(iii) Electron paramagnetic resonance spectroscopy 119
(iv) Magnetic susceptibility measurements 121
(v) Electrochemistry 122
(vi) Resonance Raman spectroscopy 123
(vii) Mössbauer spectroscopy 125
D. Photochemical studies 126
E. Concluding remarks 128
Acknowledgements 128
References 128

A. INTRODUCTION

The chemistry of transition metal cluster compounds has grown to be a major research effort in inorganic chemistry. Interest in these complexes has been motivated by curiosity, as well as by the fact that such complexes show activity toward carbon monoxide and hydrogen activation [1–14]. Furthermore, these compounds may provide stereochemical models for catalytic reactions which proceed on metal surfaces [15–22]. Of course, differences are expected [23–25].

Examples of reactions which are catalyzed by metal carbonyl or hydrido-

0010-8545/81/0000–0000/$12.50

carbonyl clusters are numerous. Recent work by Ford and co-workers has demonstrated catalysis of the water gas shift reaction by metal cluster compounds derived from $Ir_4(CO)_{12}$, $H_2Ru_4(CO)_{12}$, $H_4Ru_4(CO)_{12}$, $Rh_6(CO)_{16}$, $H_3Re_3(CO)_{12}$, and $H_2FeRu_3(CO)_{13}$ [26]. A diamine/$Rh_6(CO)_{16}$ mixture has also been examined as a catalyst for the water gas shift reaction [27]. Rhodium carbonyl cluster complexes, derived from $Rh_6(CO)_{16}$, were thought to function as catalysts in the Union Carbide process for the production of ethylene glycol from synthesis gas [28]. Catalysis by supported metal cluster compounds has also been demonstrated [29–33]. Humphries and Kaesz have reviewed the reaction chemistry and stereochemistries of transition metal hydridocarbonyl cluster complexes [34]. Reports of their catalytic activity have also appeared [15,16,35].

Knowledge about the electronic structure of transition metal clusters may provide a fundamental basis for understanding the bonding and reactivity properties of these materials. Accurate knowledge about the electronic structures of aromatic organic molecules has led to detailed theories for their thermal and photochemical reactivity. By comparison, the electronic structures of metal cluster complexes are less well defined. A number of reviews have appeared dealing with electronic configurations in transition metal clusters [36–49], but no extensive survey has appeared in the last decade. At that time, theoretical work was limited to electron counting approaches [50–55], Kettle's topological method [56–61], and simple MO calculations [62–64]. Spectroscopic data available at that time was also relatively scarce [10,11,49,65,66]. The intervening increases in computing capabilities have allowed more sophisticated calculations to be performed, such as those employing the $X\alpha$ method. Studies concerning the effect of geometrical structural changes on the electronic structure may now be performed with semiempirical approaches, such as extended Hückel theory. Application of physical techniques such as photoelectron spectroscopy has provided new experimental data concerning energies of molecular orbitals and their atomic character [67].

This review summarizes spectroscopic and theoretical investigations pertaining to the nature of the metal–metal bond in transition metal cluster complexes. Only clusters with three or more metal centers, and which display strong metal–metal interactions will be considered. We have attempted a comprehensive survey up to late 1980 and in many instances the available knowledge may be limited. There are few complexes where one can be certain about the validity of the electronic structural model. For this reason it is difficult to be critical about the various models without incorporating our prejudices. We have tended to expand the discussion of key systems where a consensus of opinion has been achieved. In most instances we defer the decision of which approach is the "best" to the reader; although our

views regarding the reliability of various theoretical models are provided in the following section. The electronic structures of dimeric species have been extensively reviewed elsewhere [68–75] and are not included in this work. Clusters where the metal atoms interact weakly through exchange interactions, as in $Ru_3OX_6L_3$ [76–79], $Cu_4OX_6L_4$ [80–82], (L = ligand) and large copper clusters [83–87] will not be reviewed. Non-stoichiometric compounds such as Cu_xS_y [88] and lanthanum halides [89] will also be excluded.

First we deal with the theoretical studies. The common methods include complete neglect of differential overlap (CNDO), linear combinations of atomic orbitals—MO (LCAO–MO), extended Hückel MO (EHMO), and $X\alpha$ calculations. A survey of the results for naked atom clusters will be included in these discussions. The spectroscopic section deals with photoelectron, optical, electron spin resonance, resonance Raman, Mössbauer, and magnetic circular dichroism spectroscopy. Magnetic susceptibility and mass spectrometry studies will be cited when relevant.

The third section highlights the photochemistry of transition metal clusters, because of the intimate relationship between electronic structure and photochemical behavior. This survey will center upon photoreactivity and not upon preparative aspects such as the formation of $M_2Fe(CO)_{14}$ (M = Mn, Re) [90–92] and $Cp_3Rh_3(CO)_2$ [93,94].

B. THEORETICAL BACKGROUND

A number of theoretical approaches to the description of the electronic properties of transition metal cluster compounds have been introduced. Although the complexity of these molecules initially restricted theoretical discourse to qualitative models, recent advances have allowed a more quantitative insight. The polyhedral skeleton electron pair theory, developed by Wade and Mingos, has been quite successful in predicting the structures of metal clusters, as had been done with boron cage compounds [50–54,95–97]. By enumerating the number of electron pairs directly involved in the metal–metal bonding, a closo-, nido- or arachno-type structure can be predicted. Recent reports have suggested, however, that the $\{BH\}_n$ systems and metal cluster compounds are not entirely analogous [98–100]. The valence bond approach has been championed by Pauling to explain trends in structures, bond energies, and bond lengths in transition metal clusters [101–105]. Other workers have claimed valence bond theory to be incapable of explaining certain features of electron deficient clusters [62,106]. The electron-in-a-box approach has been examined as a possible useful alternative [107], and ligand field theory has been applied to metal cluster complexes as well [108]. Lauher's cluster valence molecular orbital method [109,110] treats the ligands only as perturbations of the electronic configura-

tion of the metal core. In this scheme, the number of valence electrons in the cluster is used to predict the geometry of the metal framework. The application of Lauher's theory to molecular cluster species has been very successful. This approach was later modified and applied to large close-packed cluster compounds [111]. The conflicting hypothesis that the cluster geometry in metal carbonyls is directly determined by the symmetry of the close-packed CO polyhedron has also been broached. This model attempts to account for steric constraints [112,113] and minimize the non-bonding interactions [114].

The complete neglect of differential overlap technique, originally designed for organic molecules, has been adapted for heavier nuclei [115,116]. This has allowed a simple semiquantitative analysis of the electronic structure of some high symmetry clusters [117–120]. The extended Hückel approach has been the most widely used [121–126], and until the introduction of the more sophisticated Xα method [124,126], the most successful quantitative model. Excellent detailed treatments of the theoretical methods employed by inorganic chemists are available [127]. The following discussion provides only a brief introduction to the EHMO, CNDO, Fenske–Hall, and Hartree–Fock–Slater (HFS or Xα) computational procedures.

(i) Techniques

In terms of the required computational effort, EHMO remains the most economical technique. It starts with the LCAO–MO approximation and expresses the wavefunction for a metal (M)–ligand (L) bond as

$$\psi_i = a\phi_M + b\phi_L$$

For more complicated systems ϕ_M and ϕ_L are normalized symmetry adapted linear combinations of atomic orbitals that belong to the same irreducible representation of the molecular point group [128]. If there are only two such species, the secular determinant assumes the form

$$\begin{vmatrix} H_M - \epsilon & H_{ML} - S\epsilon \\ H_{ML} - S\epsilon & H_L - \epsilon \end{vmatrix} = 0$$

where ϵ, the eigenvalues, are the orbital energies (which one solves for) and S the group overlap integral. The H_M and H_L are semiempirical quantities and set equal to valence state ionization energies (VSIE's) or valence orbital ionization potentials (VOIP's). The VSIE's may be related to the charge and configuration of the M and L atoms [128]. A population analysis is then used to determine atomic charges and configurations. This procedure yields new values for H_M and H_L that are substituted back into the secular determinant. When this sequence of operations is repeated, one has the

self-consistent charge and configuration (SCCC) EHMO type of calculation. In the preceding types of computations, the H_{ML} matrix elements are usually approximated as:

$H_{ML} = (1/2)S(H_M + H_L)$, the Mulliken approximation;
$H_{ML} = (1/2)FS(H_M + H_L)$, the Wolfsberg–Helmholz approximation;
$H_{ML} = -2F(H_M H_L)^{1/2}$, the Ballhausen–Gray approximation;

where F floats somewhere between 1 and 2. The exact choice of the various parameters is something of an art, but when done properly useful results may be obtained. The limitation of this method is that one cannot reasonably expect to obtain accurate absolute transition energies from Hückel methods.

Probably the most useful application of Hückel theory is to study geometrical influences upon electronic structure. Because of the minimal computational requirements of EHMO, it is possible to sample many different geometries and predict bonding trends. Even the ab initio devotee might consider using an accurate calculation to calibrate (i.e., empirically fit) an EHMO computation for the same geometry. One could then use the latter theory to extend one's knowledge about the potential surface. Unfortunately there have been few conformational studies of large cluster complexes.

The CNDO procedure is based upon Roothann's SCF–LCAO–MO method

$$\phi_i = \sum_{r=1}^{m} C_{r_i} \chi_r$$

where the trial molecular wavefunctions, ϕ_i, are expressed as a linear combination of atomic wavefunctions χ_r and there are m atomic functions in the basis. These ϕ_i are then substituted into the Hartree–Fock equations. For a closed sheli case the eigenvalue problem assumes the form

$$\left\{ H_{\text{core}}(1) + \sum_{j=1} \left(2J_j(1) - K_j(1)\right) \right\} \phi_i(1) = \epsilon_i \phi_i(1)$$

where H_{core} includes the electron–nuclear attractive potential and the electron kinetic energy operator. Electron–electron interactions have a repulsive component due to Coulomb's law (the J_j) as well as a contribution arising from the quantum mechanical "exchange attraction" (the K_j) between electrons of the same spin. If the preceding equations are left multiplied by ϕ_j and integrated, one arrives at the matrix formulation (SCF–LCAO–MO procedure of Roothaan)

$$\boldsymbol{FC} = \boldsymbol{SCE}$$

where $\boldsymbol{F}$ is the Hamiltonian matrix, $\boldsymbol{C}$ the eigenvector matrix, $\boldsymbol{S}$ the overlap matrix and $\boldsymbol{E}$ the diagonalized eigenvalue matrix. To solve the problem one

guesses a set of coefficients for the eigenvectors of occupied orbitals, then calculates J_i and K_i potentials to yield an $\boldsymbol{F}$ and $\boldsymbol{S}$. Then solve for $\boldsymbol{E}$ to compute a new $\boldsymbol{C}$ and continue the cycle until convergence obtains. The CNDO approximation further assumes that: (1) $\boldsymbol{S}$ is the unit matrix (i.e., zero differential overlap); (2) $\langle \chi_i | H_{\text{core}} | \chi_j \rangle = 0$ unless χ_i and χ_j (individual atomic basis orbitals) are located on the same atom; (3) in the electron–electron repulsion and exchange integrals $\chi_r(1)\chi_s(1) = 0$ when $r \neq s$ (i.e., complete neglect of the differential overlap). Useful empirical expressions are available for the two center–two electron integrals and diagonal F_{rr} elements are available for first row atoms. Unfortunately, one has to calculate these quantities (generally using Slater type orbitals) for inorganic complexes. Frequently, poor results are obtained and one should cautiously employ results from a CNDO calculation. A more successful approximate SCF–LCAO–MO strategy has been developed by Hall and Fenske [129]. Diagonal $\boldsymbol{F}$ matrix elements are calculated exactly, except that the Coulomb potential due to neighboring atoms employs a point charge approximation. These charges are determined with the aid of a Mulliken population analysis. Off diagonal elements are estimated with a modified Mulliken approximation.

Local density methods were given renewed impetus by the theorem of Hohenberg and Kohn [130], that proved the electron density of a system uniquely fixes its energy and potential. The HFS or Xα approximation [131] replaces the Hartree–Fock exchange potential operator K_j with that of a free electron gas

$$[K\mathrm{X}\alpha\uparrow(1)] = -6\alpha\left[\frac{3}{4\pi}\rho\uparrow(1)\right]^{1/3}$$

where α is a scaling factor, generally fixed for an atom by making the HFS atomic electron density agree with the HF density. In most cases α is about 0.7. This equation also illustrates the origin of the name Xα (exchange alpha).

Although it has been argued [131] that Xα is superior to HF (due to inclusion of some correlation), the two theories are roughly comparable. One must not forget that even HF theory fails miserably in cases where electron correlation effects are important [132]. In practice, further approximations to the Coulomb potential are necessary to facilitate the calculation of electron–electron matrix elements. The simplest approximation, the muffin tin (MT) Xα, assumes spherical symmetry of the potential within touching spheres around each atom. In the large extra sphere volume, the potential is assumed constant [131]. Obviously, atomic environments in many molecules are not spherically symmetrical and the MT approximation is a poor one, in molecules with a strong bond, e.g., CO. The problem may be alleviated

(SCF–Xα–SW) by allowing the spheres to overlap and thereby allow some flexibility in the description of the bonding (overlapping) regions [133].

The other approach to the solution of Poisson's equation for the Coulomb energy has been to employ numerical methods to approximate the difficult integrals. This technique, called the discrete variational (DV) method [134], computes values of the functions to be integrated on a grid of 1000–10000 points distributed throughout the molecule. Numerical accuracy is determined by the density of sampling points. It is still convenient to expand the molecular charge density in spherical harmonics localized on each atom. The latter expansion may be determined by an analytical least squares fit [135] or approximated by an S wave expansion from an orbital charge-population (SCC) analysis [136]. For the theoretical purist, the DV approach offers no adjustable parameters, other than the usual basis set flexibility.

There is an important difference between an Xα and HF orbital energy scheme. An Xα orbital energy ϵ_i is the partial derivative of the total energy with respect to the occupation number η_i for that orbital. This contrasts with HF theory where a spin orbital is either occupied $\eta_i = 1$ or not $\eta_i = 0$. Consequently, the Xα ϵ_i are not expected to be equal to the HF ϵ_i. In some respects this might be a disadvantage because Koopman's theorem cannot be applied; however, Xα theory readily predicts spectroscopic energies and allows for orbital relaxation effects via the "transition state". Details of the procedure are provided elsewhere [131] and we will illustrate the principle with an example. To calculate the ionization potential for removal of an electron from orbital ϕ_i, we calculate the energy, ϵ_i, with 1/2 an electron removed from ϕ_i. Note, this corresponds to a pseudo transition state (i.e., halfway point) for electron loss. The advantage of the transition state approach is the rapid convergence of the calculation, once the ground state wavefunction has been determined.

(ii) Naked atom clusters

Naked atom clusters are plausible models for metal surfaces and crystallites [137–149]. A number of theoretical articles specifically examined the interplay between electronic structure and chemisorption on small clusters and surfaces [117,144–146,148,150–159]. Reflecting their relative importance in heterogeneous catalysis, most of these calculations have centered on the noble and group eight transition metals.

Extended Hückel MO calculations (EHMO) have been widely used in characterizing these materials. Anderson employed this theoretical approach to explain not only the photoemission from bulk copper surfaces (using Cu_{13} as the model), but also the structures and optical spectra of small (up to Cu_5) copper clusters [140,141]. He found the Cu_3 fragment to be linear and

quite stable, as has been proposed for Ni_3 [160]. The lowest energy optical transitions occur at approximately 20000 cm^{-1} and were assigned to the valence electron transitions $1s\sigma_u \rightarrow 2s\sigma_g$ and $1d\sigma_g \rightarrow 2s\sigma_u$ [140]. A "Z-shaped" configuration is predicted for the weakly bound Cu_4 cluster, which more exactly approximates two weakly interacting dimers. Pentanuclear copper is also predicted to be linear. In the higher nuclearity clusters ($\geqslant Cu_4$), specific assignments of electronic bands are difficult due to extensive overlap of the sundry transitions. Calculations on the Ni_3 and Ni_4 species shows them to be linear, barely more stable than the ring conformations [160]. The most stable structures of Ti_x, Fe_x, Cr_x and Ni_x ($x = 3$–6) clusters were computed and compared [145]. The results are summarized in Table 1. The titanium clusters appear to prefer tight structures with positively charged corners, whereas nickel adopts open, ring-like conformations with negatively charged vertices [145]. Subsequent ab initio effective core SCF calculations on small nickel clusters (up to Ni_6) confirmed the preferred configurations as determined by the extended Hückel method [161]. The greater stability of linear Ni_3 with respect to the ring conformation was attributed to Jahn–Teller destabilization in the D_{3h} geometry which leads to ring opening. In general, the nickel species could be described as arrangements of Ni atoms localized in $3d^9$ electronic configurations and bound by their 4s electrons (ca. 1 per Ni atom). Silver adopts linear chains for species

TABLE 1

Preferred geometrical configuration of some naked atom clusters as determined by extended Hückel molecular orbital calculations

Cluster	Most stable geometry (Point group)
Ti_3, Cr_3, Fe_3	Triangular (D_{3h})
Ni_3	Linear ($D_{\infty h}$) slightly preferred over triangular (D_{3h})
Cr_4, Fe_4	Tetrahedron (T_d), square (D_{4h}), and rhombus (D_{2h}) are essentially isoenergetic
Ni_4	Square (D_{4h}) slightly preferred over linear ($D_{\infty h}$)
Ti_4	Diamond (D_{2h}) over square (D_{4h}) due to Jahn–Teller distortion
Fe_5	Square pyramidal (C_{4v})
Cr_5	Pentagonal (D_{5h})
Ti_5	Triangular bipyramidal (D_{3h})
Ni_5	Pentagonal (D_{5h})
Ti_6	Octahedral (O_h)
Cr_6	Triangular Prismatic (D_{3h})
Fe_6	Hexagonal (D_{6h})

containing less than thirty atoms, beyond which a face centered cubic lattice is the most stable allotrope [137,162,163]. Baetzold has applied EHMO to metal atom clusters as large as 55 [162]. The calculated ionization potentials and electron affinities approach those known for the bulk metals. In general, the calculated IP's are greater and the EA's less than those of the surface. Bond energies also tend to be lower for the clusters and they bind substrates less well than the extended metal [162,163]. The calculations attempt to rationalize catalytic activity based upon the electronic properties of isolated metal clusters.

Hartree–Fock calculations for nickel species up to Ni_{87} indicate that the IP converges to the bulk value by Ni_{43}; however, the cluster EA's are low (2.5 eV) even for Ni_{87} [164]. Conduction bandwidths are similar (ca. 16 eV) in both the bulk metal and clusters larger than 80. The electron density at the surface atoms is significantly lower than bulk nickel, which may explain the differences in chemisorption and catalytic properties. Differences in the electronic properties of fine metallic particles versus bulk metal have been defined [24,25,165]. The small clusters show greater paramagnetic susceptibility, smaller heat capacities, and slower relaxation processes. Copper microcrystals have been found to exhibit geometric disorders and bond length anomalies as well [140]. In addition, small naked metal atom clusters have very large spacings of energy levels [24].

Matrix optical spectra of small silver clusters have been discussed, employing EHMO calculations on Ag_3 and Ag_4 fragments [166]. The results were deemed inadequate for an accurate assignment of electronic transition energies. These authors questioned the ability of previous workers [167] to make definitive statements concerning the assignment of a certain band to a particular cluster. Mixed chromium–silver trimers have been isolated and their optical spectra elucidated with the use of the EHMO method [168]. Anderson has also explained the matrix shifts observed in the optical spectra of small Cu and Ni clusters as a result of antibonding interactions between the metal's $4s$ and $4p$ levels and the argon's $3p$ orbitals [140,160]. A qualitative crystal field rationale also accounts for the observations [169,170]. In light of the ability of EHMO to determine ground state geometries and properties, the procedure was recently defended [141] against criticisms that it was (1) more inaccurate, and (2) more parameter dependent, than the $X\alpha$ method [125,126].

Chemisorption and its effect on electronic structure have been examined by Anderson and Hoffmann [152]. They arrived at the following conclusions regarding the surface-substrate interaction:

(1) Charge transfer occurs upon chemisorption of adsorbate in accordance with the relative electronegativities.

(2) Adsorbed molecules tend to dissociate due to Coulombic repulsions

that result from filling the antibonding orbitals.

(3) There are strong attractive interactions between adsorbate and substrate which are independent of orientation.

(4) Step and corner sites exhibit the strongest substrate binding. This had also been found previously in work that employed less elaborate models [148,149,157].

(5) EHMO calculations can explain the photoemission of adsorbed molecules on W(100) and Ni(100).

Anders et al. investigated H and N adsorbed on W_9 clusters to model W(100) in the same fashion as above [150,151]. The preferred binding site was 5 coordinate. The net W–N bond order in that site was 2.85. Hückel calculations for N_2 on a trimetal fragment have also been reported [171]. Chemisorption of 5*d* transition metal atoms (M) on a tungsten surface has been modeled by $W_4(\mu_4\text{-M})$ [154–156]. Using CNDO and extended Hückel theory, the bonding was described in terms of a surface molecule. Hamiltonians developed by Anderson [172] and Hubbard [173,174] were employed to give a more elaborate description. Adsorption was predicted to be predominantly neutral.

Catalytic activity and hydrogen solubility of nickel, palladium, and platinum have been related to the properties of H adsorbed on small clusters. Metal–hydrogen bonding is dominated by the *d* orbitals in Pd and Pt, but in the case of Ni, the 4*s* orbital is most important [175–177]. It had been previously thought that *d* orbitals dominated substrate binding on most surfaces [178,179]. A CNDO–MO calculation of H on a Ni_{10} unit shows the hydrogen to be most stable when located directly over a hole site in the nickel surface [117,176]. The binding energy was computed to be 73 kcal $mole^{-1}$, in good agreement with experimental measurements of 67 kcal $mole^{-1}$ [180]. Much less stable (26 kcal $mole^{-1}$) was the placement of hydrogen directly over a nickel atom. The importance of the Ni 4*s* and 4*p* orbitals in the metal–hydrogen bonding was emphasized, as the hydrogen assumed some negative charge; however, these results do not agree with earlier EHMO calculations that favor a hydrogen directly above a nickel atom [176]. Another EHMO study supported the CNDO results, showing the H over a hole to be 7 kcal $mole^{-1}$ more stable than that directly above a metal atom [181]. Calculations for isostructural copper clusters indicated an even stronger contribution from the metal 4*s* orbital [176]. Thus, it would appear that Ni and Cu clusters utilize significantly more metal *s* orbital character when binding substrates than do their heavier cogeners. Van Dyke also looked at H chemisorption on Cu and Pt. No clear-cut conclusions could be made concerning the electronic properties of these materials [153]. Some $X\alpha$ calculations on the Pd_6 and HPd_6 clusters have been reported and the predicted core level shifts upon H binding agree with the XPS data [182].

One of the more popular subjects for atomic cluster calculations has been CO binding to small nickel clusters. Hückel calculations for planar Ni_8 and Ni_{15} with CO revealed asymmetrical bridge binding of CO to two nickel atoms [183]. In contrast with earlier studies [184,185], there was a slight preference for terminally bound CO over the bridged isomer [183,184]. A CNDO calculation for a planar Ni_{10}–CO cluster attempted to assign the photoelectron spectrum [118]. Although the quantitative agreement was poor, the predicted spectral band shape was correct. Unlike other calculations [183,186,187], this study claimed that the surface-CO binding energy was insensitive to orientation. The binding of CO to Ni_{2-5} clusters has been examined with the Xα method [188,189]. Contrary to earlier work [190,191], the importance of Ni 4*s* and 4*p* orbitals was demonstrated. Energy levels for Ni_4CO and Ni_5CO closely resemble the PES of CO on the Ni(100) surface [189]. Ellis and co-workers have performed a HFS study of Ni_5CO [186,187]. They noted the similarity to the PES of CO on Ni(100) and computed the binding energy as a function of the CO to surface distance.

The energetics of CO binding to small iron clusters has also been carried out using the EHMO approach [192]. The calculated energy for the iron–carbon bond was estimated at 29 kcal mole^{-1}. A planar Fe_9 cluster was used as the model. Employing a simpler linear metal cluster gave a much higher value (42 kcal mole^{-1}), indicating a three-dimensional cluster would be the best approximation of the surface. Studies on Fe_{13}(CO) gave bond energies comparable to that for Fe_9(CO). The preferred coordination site appears to be triply bridging instead of terminal [192]. The results were compared with experimental data and simpler model systems.

The Xα method has been used primarily in the study of chemisorption effects, although Yang and Bambakzdis have carried out calculations on the naked Pd_{13} cluster [163]. Rösch and Menzel examined hexanuclear silver, nickel, and copper clusters and found similar bandwidths and *d*-band/Fermi level gaps as those in the bulk metals [144]. Studies on large iron clusters achieve the same degree of accuracy with regard to magnetic as well as electronic properties of the metal [193]. Small silver clusters, Ag_n ($n = 2$–6), have been examined by Xα techniques and the resulting energy diagrams used to aid the assignment of optical transitions [194]. Octahedral species such as Nb_6, Mo_6, W_6, and Ta_6 show electronic properties approaching those of the bulk metals [195]. Investigation of size effects in the niobium series indicated that an increase in the number of atoms increases the bandwidth while decreasing the energy of the Fermi level. An interpretation of the photoemission spectrum of oxygen on Ag(100) was derived from a calculation of Ag_4O [144]. Shifts in the UPS spectra of analogous Ni_4O and Cu_4O species were rationalized. A similar calculation on these clusters by Head et al. supported these conclusions [196]. In the Ni_5O system, oxygen prefers a

fourfold site and the computed energy diagram corresponds well with the He(I) photoelectron spectrum [196]. The Xα calculation of O_2 and CO on Pt_5 shows partial dissociation of O_2 into oxygen atoms upon adsorption [197], whereas CO remains intact. The carbon monoxide should preferentially occupy a hole site on the platinum surface, in agreement with SIMS studies [198]. A paper describing the electronic structure of Ni_4S has also appeared [199].

Other approaches have been presented. Gaspard used a tight-binding model in his calculations of Cu_{13} [200]. Bullett and O'Reilly developed a pseudopotential to ease the computational demand, and demonstrated its applicability to small cluster systems [142]. In accordance with other studies, the addition of metal atoms to the cluster broadened the *d*-band and decreased the gap to the Fermi level. It is interesting that the electronic structure of coordinated CO was nearly indistinguishable whether terminal or bridging [142].

(iii) Trinuclear cluster complexes

The work on trinuclear clusters has centered on the metal carbonyls $M_3(CO)_{12}$ where M = Fe, Ru, and Os and the rhenium halides $Re_3X_{9+n}^{n-}$ ($n = 0-3$) (see Figs. 1 and 2). These complexes are attractive candidates for theory because of the availability of large amounts of experimental data, especially photoelectron spectra, and the metal–metal interactions appear to be strong.

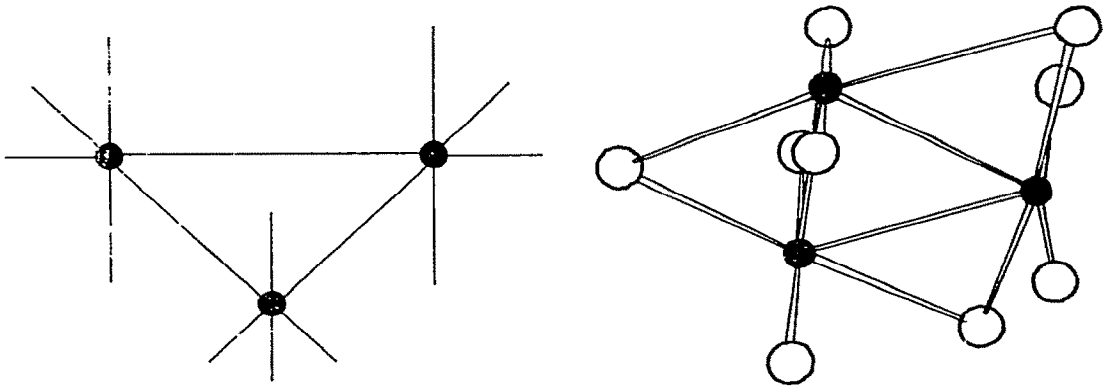

Fig. 1. Molecular structure of $M_3(CO)_{12}$ (M = Ru, Os).

Fig. 2. Molecular structure of Re_3X_9 (X = Cl, Br).

A simple LCAO–MO calculation was employed to derive a qualitative energy diagram for the *d*-derived molecular orbitals in Re_3^{9+} [62]. The symmetries of both the LUMO and the HOMO were predicted to be e''. This was offered as a model for Re_3Cl_9 and it was claimed that valence bond theory and its 2 electron–2 center approach could not account for the bonding without introducing awkwardly bent bonds, ad hoc assumptions, or unpaired electrons. Ferguson et al. adopted a similar approach to Re_3Cl_9, and emphasized the importance of metal–metal π type orbitals to account for the very short rhenium–rhenium bond lengths [63]. Korol'kov and co-workers have also performed a series of MO calculations of these compounds [201–203]. They found the σ and π contributions to the Re–Re bond to be equal [201]. A list of calculated bond energies for the chloride and bromide systems is given below (see Table 2). The agreement with thermodynamic and mass spectral data is said to be good [202]. The bromide cluster was predicted to have stronger metal–metal bonding, but weaker metal–ligand bonds.

Recently, the SCF–Xα–SW method has been applied to Re_3Cl_9 and $Re_3Cl_{12}^{3-}$ [204] (see Fig. 3(B)). In agreement with qualitative predictions, the HOMO was found to be e'' with approximately 60% metal character. The LUMO was of a_1'' symmetry, and permitted assignment of the two lowest energy bands in the electronic spectrum of $Re_3Cl_{12}^{3-}$ [204]. Discrete variational Xα calculations have been reported [205] for Re_3Cl_9 and $Re_2Cl_8^{2-}$ [205] (see Fig. 3(A)). An interesting qualitative feature of these studies was the stability of $3a_1$, the cluster σ bonding level, which has the metal–metal bonding lobes directed toward the center of the trirhenium core. This strong interaction would be expected to weaken bonds that could be formed at the vertices of the triangle, and would explain why additional ligands, L, in $Re_3X_9L_3$ compounds, are not bound tightly [205]. Bursten et al. incorporated relativistic corrections in their SCF–Xα–SW calculation [206] (see Fig. 3(C)). They also carried out a Fenske–Hall type calculation that gave a slightly different energy level diagram (see Fig. 3(D)). These data were used to rationalize photoelectron and electronic spectra [206].

TABLE 2

Calculated bond energies (kcal mol^{-1}) in Re_3X_9 (X = Cl, Br) cluster compounds

Bond	Re_3Br_9	Re_3Cl_9
Re–Re	103	85
μ–Re–X–Re	73	90
Re–X (terminal)	58	72

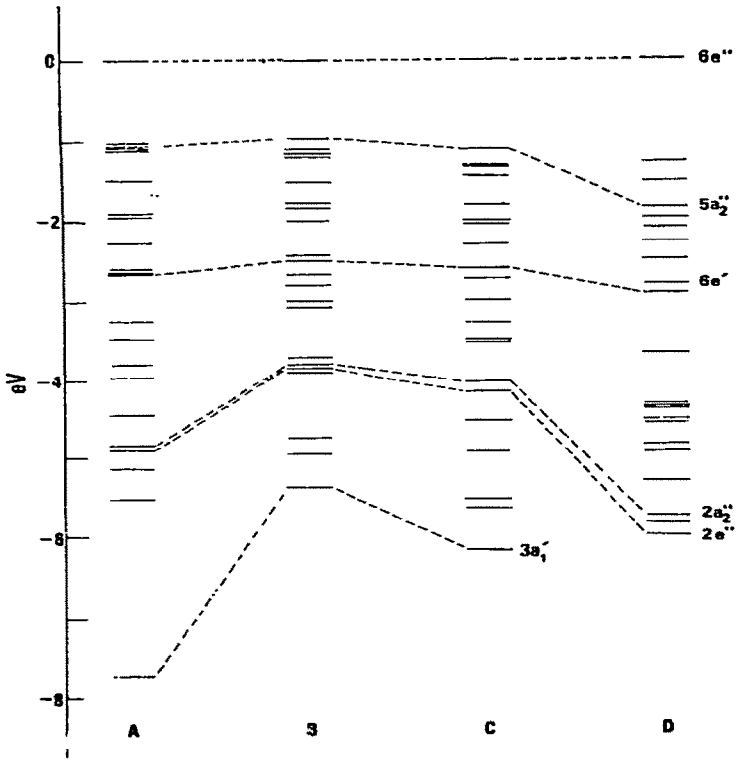

Fig. 3. Calculated energy diagrams for Re_3Cl_9. (A) SCC–Xα–DV calculation. (B) SCF–Xα–SW calculation. (C) SCF–Xα–SW calculation with relativistic corrections incorporated. (D) Fenske–Hall calculation. The highest occupied molecular orbital has been adjusted to 0 eV for comparative purposes. Only metal localized orbitals are labelled.

Fenske–Hall and various Xα calculations of Re_3Cl_9 are compared in Fig. 3. The reasonable agreement between the three Xα calculations is encouraging. Predominant metal–metal bonding orbitals are connected by dashed lines in the figure. All Xα studies concur on the nature of shallow valence orbitals apart from minor ($\pm$0.5 eV) shifts. More significant differences are found among the deepest occupied valence orbitals. Although there is a consensus on the relative ordering, the absolute orbital energies differ substantially ($\pm$2 eV). Considering the differing treatment of core electrons in the three studies, this may not be so unreasonable. Unfortunately, the published photoelectron spectra are not particularly informative in this spectral region. Major qualitative discrepancies occur between the Xα and Fenske–Hall models for Re_3Cl_9 and the UV photoelectron data appears to be more consistent with the Xα scheme.

TABLE 3

Estimated force constants for metal–metal stretching modes in some small metal carbonyl clusters

Cluster	Metal–metal force constant (N/m)
$Ru_3(CO)_{12}$	83
$Os_3(CO)_{12}$	106
$H_3Mn(CO)_{12}$	37
$Co_4(CO)_{12}$	54 [a]
$Rh_4(CO)_{12}$	81 [a]
$Ir_4(CO)_{12}$	159

[a] For non-bridged bond.

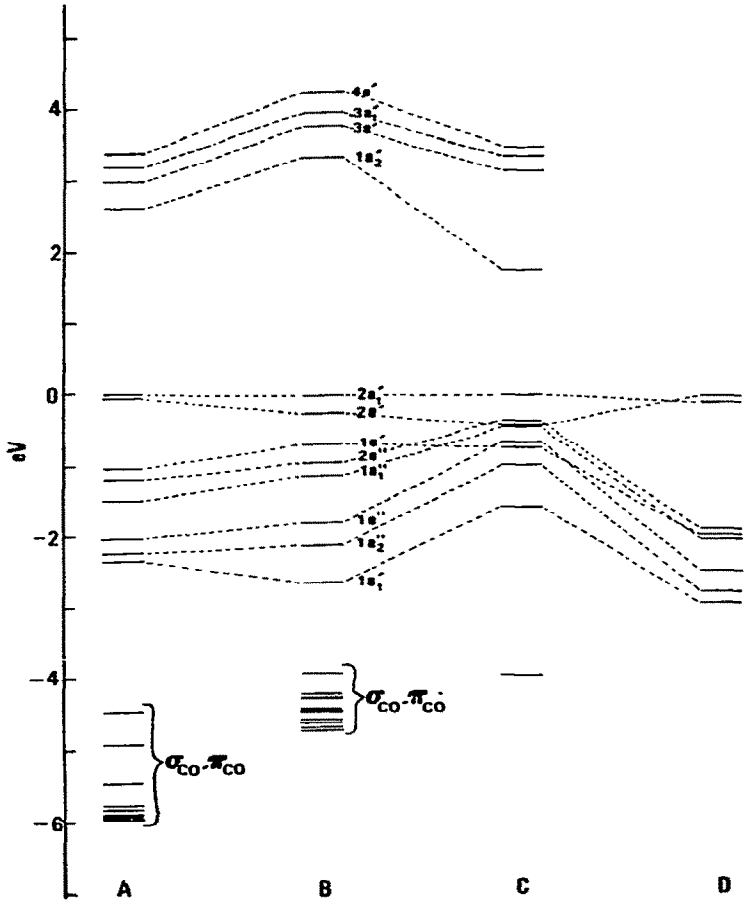

Fig. 4. Calculated energy diagram for $Ru_3(CO)_{12}$. (A) Xα–DV calculation using a multipolar potential. (B) SCC–Xα–DV calculation. (C) Extended Hückel MO calculation. (D) Complete neglect of differential overlap model calculation. The highest occupied molecular orbitals have been adjusted to 0 eV for comparative purposes.

The first molecular orbital calculation for a metal cluster was performed on $Fe_3(CO)_{12}$ [207]. A linear geometry, as proposed by Sheline [208], was used instead of the correct triangular arrangement of metal atoms [209,210]. Korol'kov and Miessner were the first to consider the electronic structure of a triangular $M_3(CO)_{12}$ cluster, $Os_3(CO)_{12}$ (see Fig. 5(C)) [211]. Their calculations predicted force constants for the metal–metal and metal–carbon bonds, bond orders, dissociation energies, and first ionization potentials [203,211]. Normal coordinate analyses of the simple trinuclear carbonyls $Ru_3(CO)_{12}$ and $Os_3(CO)_{12}$ as well as the $M_4(CO)_{12}$ clusters (M = Co, Rh, Ir) have predicted force constants for the metal–metal bonds (see Table 3) [212]. A good correlation was found between their calculated bond orders and known bond distances. Employing the CNDO method, an energy diagram was derived and used to explain the photoelectron spectrum of $Ru_3(CO)_{12}$ [119] (see Fig. 4(D)). Tyler et al. studied the electronic structure of all the $M_3(CO)_{12}$ clusters (M = Fe, Ru, and Os) [213]. An EHMO calculation, performed on the $Ru(CO)_4$ fragment, was used to construct an energy level diagram for $Ru_3(CC)_{12}$ (see Fig. 4(C)). Three allowed transitions to the metal–metal σ^* orbital were predicted. Assisted by spectroscopic techniques such as magnetic circular dichroism and polarized single crystal studies, a complete assignment of the electronic spectrum was proposed (see Table 4). The $Os_3(CO)_{12}$ spectrum was analyzed similarly, postulating stronger metal–metal interactions and, therefore, a larger bonding–antibonding splitting.

Recent Xα calculations concur with the assignment for the lowest allowed electronic transition ($2e' \rightarrow 1a_2'$) in $Ru_3(CO)_{12}$ (see Fig. 4(A),(B)) [214]. For the second allowed transition the $2a_1' \rightarrow 3e'$, one electron excitation is

TABLE 4

Electronic spectral data for trimetal dodecarbonyl systems

Complex	λ_{max} (nm)	$\epsilon \times 10^{-4}$	Assignment [a]
$Ru_3(CO)_{12}$	390	0.64	$\sigma \rightarrow \sigma^*$
	320 sh		$\sigma^{*\prime} \rightarrow \sigma^*$
	270 sh		
	238	3.50	MLCT
$Os_3(CO)_{12}$	385 sh	0.36	$\sigma^{*\prime} \rightarrow \sigma^*$
	330	0.86	$\sigma \rightarrow \sigma^*$
	280 sh		
	240	2.48	LMCT
$FeRu_2(CO)_{12}$	470 sh		$\sigma^{*\prime} \rightarrow \sigma^*$
	390	0.88	$\sigma \rightarrow \sigma^*$

[a] As given in ref. 79.

expected to be slightly lower in energy than $1e' \rightarrow 1a_2'$. This result is at odds with the high placement of $3e'$ (and hence the $2a_1' \rightarrow 3e'$ transition) by the EHMO computations. Good experimental data has only been obtained for the lowest energy electronic transition which must conform to $1A_1' \rightarrow 1E''$. Resonance Raman spectra exhibit enhancement of the a_1' cluster breathing mode, as might be anticipated for a metal–metal antibonding excited state. Consistent with these results, the $1a_2'$ orbital was predicted to be a cyclopropane-like σ^* orbital composed of in-plane Ru $4d$ and $5p$ character. In addition, the wavelength dependence of the Raman spectrum evidenced a

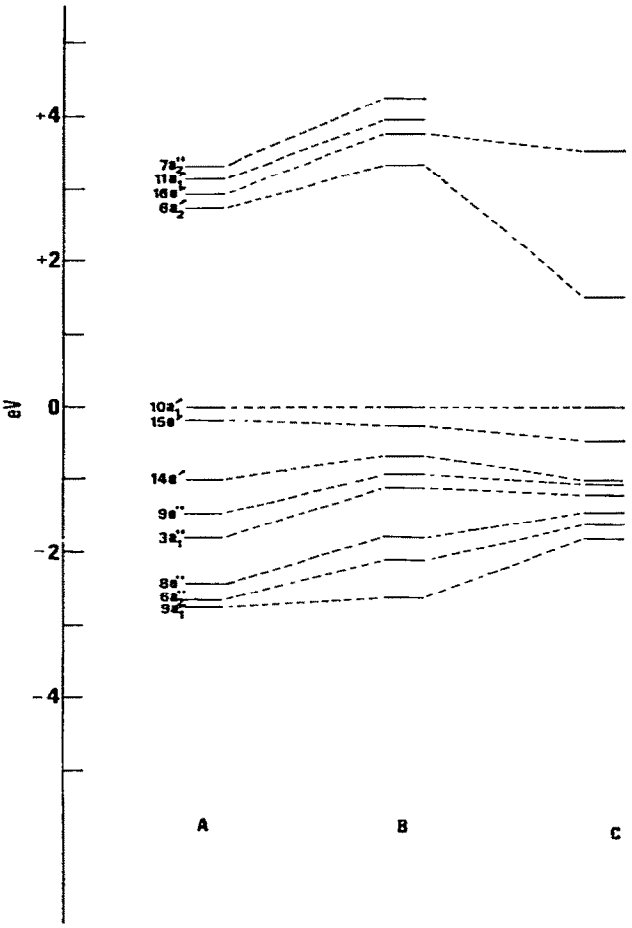

Fig. 5. Calculation energy diagrams for $Os_3(CO)_{12}$. (A) Xα–DV calculation using a multipolar potential ($L = 1$). (B) SCC–Xα–DV calculation. (C) Extended Hückel MO calculation. The highest occupied molecular orbitals have been adjusted to 0 eV for comparative purposes. The occupied orbitals shown are all metal localized.

Jahn–Teller distortion, consistent with the degenerate nature of the excited state. A similar energy diagram to $Ru_3(CO)_{12}$ was calculated for $Os_3(CO)_{12}$ (Fig. 5), with an identical ordering of metal-localized orbitals, but the ordering of electronic transition energies differs. The case of $Fe_3(CO)_{12}$ is not clear due to the presence of bridging carbonyls. There are additional bands in the electronic spectrum of the latter complex, which are as yet unassigned. The EHMO approach was applied by Schilling and Hoffmann to the hypothetical D_{3h} iron analog [215]. The HOMO was found to be a_1' in symmetry and three center metal–metal bonding in character. The same type of energy diagram was derived for the carbon tricobalt cluster compound, $Co_3(CO)_9CH$ [215]. A number of other M_3L_9 (ligand) clusters have been considered and the isolobal nature [50–52,216–222] of various ligands discussed. Evans considered the hypothetical $Fe_3(CO)_9$ and $Co_3(CO)_9$ compounds via EHMO in order to examine compounds based on these cores [223]. His method of computing $Co_3(CO)_9$, combining three $M(CO)_3$ fragments, was compared to results obtained by considering the M_3 core first and then adding nine carbonyls. Evans found the two methods gave essentially the same picture, but warned that care must be taken with the second approach. The geometry of the incoming carbonyls appears to be especially critical. Distortions in this superstructure may well alter the occupation of certain levels, as shown for $Ni_5(CO)_{12}^{2-}$ [223].

Dahl and co-workers have studied numerous organometallic chalcogenide complexes by single crystal X-ray diffraction, and have taken a special interest in trinuclear cobalt carbonyl complexes with sulfur ligands [224–227]. The cluster, $Co_3(CO)_9S$, is isostructural with the well known $Co_3(CO)_9CX$ compounds mentioned above, except that it possesses one extra electron. A simple LCAO–MO calculation shows that the additional electron may reside in either an e or a_2 orbital. Occupation of an e orbital would be expected to cause a Jahn–Teller distortion, which is not detected in the crystal structure [224,225]. The electron was thus assigned to the a_2 orbital and this was supported by single crystal ESR measurements [225]. This electron resides in a strongly metal–metal antibonding orbital, and accounts for the long cobalt–cobalt distances. The structure of $FeCo_2(CO)_9S$, which has one less electron than $Co_3(CO)_9S$, displays much shorter metal–metal bond lengths, consistent with loss of the antibonding electron [224,226]. The same qualitative MO diagram should be valid for $Co_3(CO)_3(\mu_2\text{-}SC_2H_5)_5(\mu_2\text{-}CO)$, which has two electrons in the a_2 orbital [227]. The diamagnetism of the compound again suggests that the a_2 orbital is filled instead of the e antibonding one. Applying Coulson's definition of bond order in the molecular orbital scheme [228], the cobalt–cobalt bond order is $+2/3$, whereas valence bond theory predicts a bond order of one.

Semi-empirical LCAO–MO techniques have found widespread usage.

Vahrenkamp et al. examined another cluster containing sulfur ligands, $S_2Ni_3Cp_3$ [229]. The odd electron in this system occupies the highest antibonding orbital, again making the bond lengths longer than expected. Bullett examined the Nb_3I_8 cluster using LCAO–MO for an isolated molecule as well as a band calculation for the solid [230]. The MO calculation showed six electrons in metal–metal bonding orbitals, and one electron in a localized high energy state. Due to orbital symmetry, this level cannot delocalize to other clusters, explaining its non-metallic conductivity behavior in the crystalline state. The density of states computed in the band calculation showed the same basic features, with a wide valence band (ca. 5 eV) and a large energy gap between the HOMO and the *d*-band. Cotton used simple LCAO–MO methods to describe the bonding in oxide clusters such as $Mo_3O_8^{4-}$ [231]. Each Mo^{IV} atom has two electrons available for cluster bonding, indicating the presence of single σ bonds. The HOMO is of a_1 symmetry, just above an *e* level, and rationalizes the observed diamagnetism. Cartwright et al. [232] employed Lauher's CVMO method [109,110] to explain the electronic structure of the 44 electron species $Pd_3(PPh_3)(\mu\text{-}PPh_2)_3^+$. This method assigns a formal oxidation state of zero to one palladium and of two to the others. It is clear that in this symmetrical cluster only average oxidation states are appropriate [232]. Walsh diagrams and orbital energy schemes have been derived for $Cp_3Rh_3(CO)_2$ employing Hückel theory. Mixed metal clusters such as $Fe_2Rh(CO)_{10}^-$ were treated in like fashion [233].

(iv) Tetranuclear cluster complexes

Using the LCAO–MO method, Trinh-Toan et al. have derived a qualitative energy diagram for $Fe_4X_4Y_4$ (X = triple bridging ligand; Y = non-bridging ligand) compounds (see Fig. 6) [234,235]. In $Fe_4(CO)_4Cp_4$, both the bonding and non-bonding levels are filled and the antibonding states are completely empty [234]. This would predict six single iron–iron bonds in the Fe_4 tetrahedron and the structure corroborates the prediction. Oxidation of the cluster takes an electron out of a non-bonding orbital and the bond lengths, in fact, do not change significantly [234]. The species $Fe_4S_4Cp_4$ has eight additional electrons (μ_3-S is a four electron donor: μ_3-CO is a two electron donor) so four of the metal–metal bonds are effectively negated. The structure shows two Fe–Fe distances of 2.65 Å (bonding) and four distances of 3.36 Å (non-bonding) [235]. Gall et al. performed a Fenske–Hall calculation on $Fe_4S_4Cp_4$ and $Fe_4S_4(NO)_4$ [236]. The nitrosyl cluster, having the same electron count as $Fe_4(CO)_4Cp_4$ was expected to possess a completely bonding metal core. The results for $Fe_4S_4Cp_4$ were qualitatively identical to those given above by the LCAO–MO method. A further

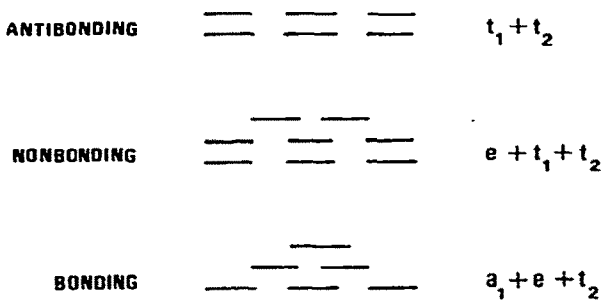

Fig. 6. Qualitative energy diagram for $Fe_4X_4Y_4$ type compounds (X = triply bridging ligand; Y = terminal ligand).

examination of these types of clusters was made by Yang et al., who performed SCF–Xα–SW computations for $Fe_4S_4(SCH_3)_4^{2-}$. Their results were used to interpret the optical spectrum of that complex [237]. The spectrum exhibited a low energy (650 nm) *d–d* transition with sulfur to iron charge transfer transitions in the near UV.

Korol'kov and Miessner have used EHMO to produce an energy diagram for $Ir_4(CO)_{12}$ (see Fig. 7(A)) [211,238]. The stabilization energy of the Ir–Ir bond was estimated to be approximately 31 kcal. The calculation also provided force constants, bond orders, and ionization potentials [211]. The natures of the HOMO and LUMO were described as strongly metal–metal bonding and antibonding, respectively [238]. Freund and Hohlneicher applied CNDO to isoelectronic $Co_4(CO)_{12}$, and a comparison of the energy diagram with that of $Ir_4(CO)_{12}$ can be seen in Fig. 7 [239]. The two compounds differ in structure, however, as $Ir_4(CO)_{12}$ possesses tetrahedral symmetry whereas $Co_4(CO)_{12}$ has only C_{3v} symmetry (see Fig. 8). The calculation considered both point groups for $Co_4(CO)_{12}$. A Mulliken charge density analysis placed approximately three times as much charge on the apical cobalt as on the basal metal atoms in the C_{3v} structure. The electronic structure of $M_4(CO)_{12}H_n$ and $M_4Cp_4H_n$ ($n = 3$, 4 or 6) has been investigated by EHMO calculations on the saturated $M_4(CO)_{12}$ and M_4Cp_4 fragments, with the hydrogens then considered as perturbations [240]. For the $Cp_4Ni_4H_3$ cluster, which contains three face bridging hydrides [241,242], there are three unpaired electrons [243]. The calculation places them in nearly isoenergetic orbitals ($a_2 + e$), which comprise a t_1 orbital in the parent Cp_4Ni_4 compound. An explanation for the variable location of the hydrogen atoms in these clusters was presented.

The LCAO–MO approach has been applied to platinum metal clusters as well. A simple MO calculation on $Pt_4(CO)_5\{P(C_6H_5)(CH_3)_2\}_4$ predicted five metal–metal bonds to be present in the Pt_4 tetrahedron [244]. The crystal

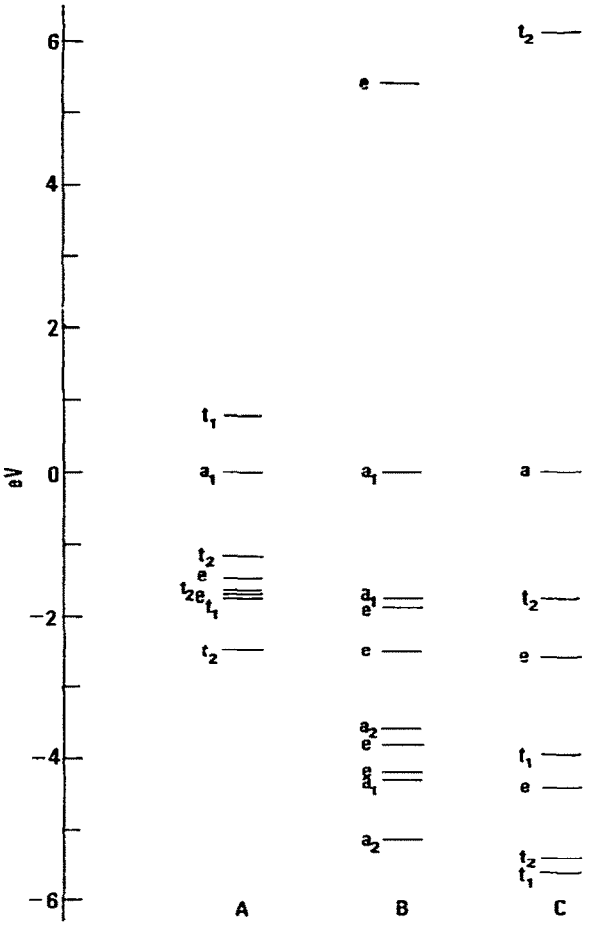

Fig. 7. Calculated energy diagrams for $M_4(CO)_{12}$ cluster compounds (M = Co, Ir). (A) Extended Hückel MO calculation on $Ir_4(CO)_{12}$. (B) CNDO calculation on $Co_4(CO)_{12}(C_{3v})$. (C) CNDO calculation on $Co_4(CO)_{12}(T_d)$. The highest occupied molecular orbitals have been adjusted to 0 eV for comparative purposes.

structure revealed five of the bond lengths to be approximately 2.75 Å, with one edge at 3.35 Å; this supported the presence of a single non-bonding Pt–Pt interaction. The addition of two electrons would yield a totally bonding metal core as predicted for $Ni_4(CO)_9^{2-}$. A qualitative MO picture of the isoelectronic cluster, $Ni_4(CO)_6\{P(CH_2CH_2CN)_3\}_4$, showed 6 metal–metal single bonds and an empty orbital available for $p \rightarrow$ Ni π backbonding [245]. The equality of Ni–Ni bond lengths concurs with this description.

The nature of gold(I)–gold(I) interactions was examined by LCAO–MO in the tetramer $Au_4(CH_3CSS)_4$ [246]. All the bonding and antibonding orbitals are filled, yielding a metal–metal bond order of zero; however, it

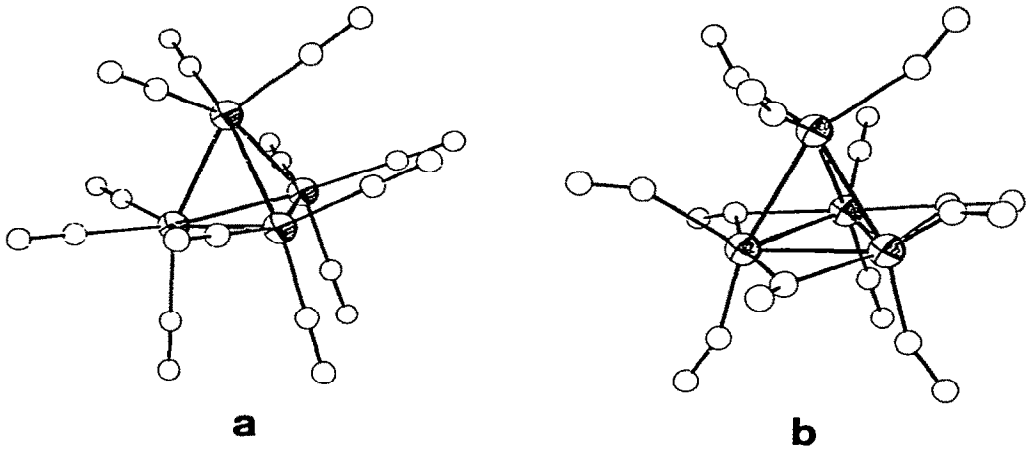

Fig. 8. (a) Molecular structure of $Ir_4(CO)_{12}(T_d)$. (b) Molecular structure of $Co_4(CO)_{12}(C_{3v})$.

was argued that the ability of the dithioacetate ligand to accept some π-electron density from the antibonding levels allows a net attractive interaction. Similar reasoning has previously been used to explain metal–metal bonding interactions between d^8 or d^{10} metal centers in binuclear metal complexes [247–251]. A final example belonging to the tetranuclear class would be Mo_4I_{11} [252], for which an MO model predicts a totally bonding Mo_4 core.

(v) Pentanuclear cluster complexes

Due to the rarity of pentanuclear clusters, there have been few theoretical or spectroscopic investigations of these complexes. Dahl and co-workers have looked at two complexes with X-ray diffraction techniques supplemented by qualitative LCAO–MO discussions. The $Ni_3(CO)_6\{M(CO)_5\}_2^{2-}$ cluster (M = Cr, Mo, W) can be thought of as the $Ni_3(CO)_6^{2-}$ cluster bound to two $M(CO)_5$ radicals [253]. The nickel trimer has 3 single bonds and two electrons delocalized above and below the ring. These electrons can match up with the unpaired electrons of the two radicals to form two delocalized 2 electron/4 center bonds [253]. The other complex, $Cp_4Ni_5S_4$, contains a

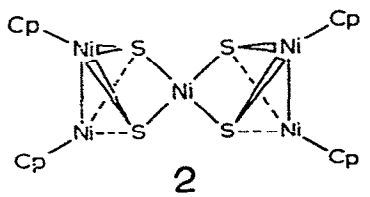

2

square planar Ni(O) atom (2). There appear to be single bonds between the outside nickel atoms, but no direct metal–metal bonding to the central nickel, according to both the geometrical and theoretical data [254].

(vi) Hexanuclear cluster complexes

Large clusters pose a tremendous computational challenge and there have been few studies that employ advanced theoretical methods. Hexanuclear clusters which received early attention were the metal halides $M_6X_{12}^{2+}$ (M = Nb, Ta) and $M_6X_8^{4+}$ (M = Mo, W). A framework LCAO–MO type calculation on $Mo_6Cl_8^{4+}$ found the 24 electrons available for metal–metal bonding to completely occupy bonding levels [62]. This gave twelve single σ bonds, or a totally bonding Mo_6 cluster. The ground state configuration was assigned as $a_{1g}^2 t_{1u}^6 t_{2g}^6 e_g^4 t_{2u}^6$, and the LUMO was of e_g symmetry. Crossman et al. had earlier considered $Mo_6X_8^{4+}$ with a vague qualitative "hybrid orbital" model [255]. Korol'kov and Pak reported EHMO calculations on both the molybdenum and tungsten species, from which they attempted to estimate metal–metal bond energies and effective charge densities [256,257]. The MO approach of Guggenberger and Sleight gave an e_g HOMO in contrast to the other calculations [258]. More recently SCF–Xα–SW calculations have been reported for these complexes [204]. The calculated energy diagrams verify the presence of a totally bonding M_6 core. The HOMO ($5a_{1g}$)–LUMO ($2e_u$) energy gap was placed at approximately two electron volts. The Xα calculation was also used to predict the optical spectrum and the agreement with experiment was reasonably good [204]. A more recent SCF–Xα–SW calculation correctly predicted the band shapes and energies in the valence shell XPS spectrum [259].

Niobium and tantalum clusters $M_6X_{12}^{2+}$ (X = Cl, Br), as well as the $M_6X_8^{4+}$ compounds, have been cited as examples of electron deficient complexes which are difficult to describe by the two center–two electron valence bond approach [106,260]. Robin and Kuebler predicted a $t_{1u}^6 t_{2g}^6 e_u^4$ ground state [64]. They also pointed out an error in the previous calculations of Cotton and Haas. Robin and Kuebler further proposed assignments for the electronic spectra of $Nb_6Cl_{12}^{2+}$ and $Nb_6Br_{12}^{2+}$ as well as for the oxidized tantalum clusters $Ta_6X_{12}^{4+}$ (X = Cl, Br). Voronovich and Korol'kov later obtained a different ground state configuration using EHMO [261,262]. The last two electrons occupy a degenerate e_g orbital ($t_{1u}^6 t_{2g}^6 a_{1g}^2 e_g^2$) in this calculation. Bond strengths between metal centers were calculated with the Ta–Ta bond (27 kcal) being slightly stronger than the Nb–Nb bond (25 kcal); however, the numbers are suspect in view of the many approximations. The approach of examining the metal core and ligands separately (instead of the joining of isolobal ML_n fragments) was adopted by Müller, who was able to

explain the magnetic properties of these compounds [263]. Müller predicted the two highest occupied orbitals as doubly degenerate and completely filled ($a^2t^6e^4e^4$ type). This would explain the observed TIP phenomenon, but it does not agree with any of the other studies [263]. Edwards et al., investigated the $Nb_6X_{12}^{4+}$ cluster, which possesses two fewer electrons. They assigned the ground state as $t_{1u}^6t_{2g}^6a_{2u}^2$ or $t_{1u}^6t_{2g}^6a_{1g}^2$ [264], which would be more consistent with the earlier predictions [62,261,262]. Wirsich employed a one-center model in work with $Nb_6Cl_{12}^{4+}$ [265]. His energy diagram gave the ground state as $t_{1u}^6t_{2g}^6a_{1g}^2$.

A small number of other hexanuclear clusters have been studied. Mingos used the Wolfsberg–Helmholz MO technique on $Co_6(CO)_{14}^{4-}$, an 86 electron system which is isoelectronic with $Rh_6(CO)_{16}$ [266]. The electronic structure is a closed shell configuration ($\cdots t_{2u}^6t_{1g}^6a_{2g}^2$) and has no antibonding orbitals occupied, thus producing a completely bonding octahedral Co_6 core. The antibonding orbitals appear to be of approximately the same character as those in $B_6H_6^{2-}$, and lends validity to Wade's analogies between boron cage compounds and transition metal clusters [50,51]. Mingos then proposed an explanation for these rules and their shortcomings [266]. Similar calculations on M_6H_6 clusters (M = Co, Ir) were used to rationalize the geometries of $Os_6(CO)_{18}$ and $Os_7(CO)_{21}$ [267]. Much of this paper applied polyhedral skeletal electron pair theory [50–54] to predict the symmetry of the metal core in these types of compounds. Another paper on $Os_6(CO)_{18}$ appeared recently and employed the frontier molecular orbital strategy [268]. The work was based on an earlier FMO calculation on $Pt_6(CO)_{12}$ [269]. The transition from the metal centered HOMO ($16e'$) to the π^* orbitals of CO was predicted to be at 2.6 eV (21000 cm^{-1}). The computed HOMO–LUMO gap was only 1 eV.

A simple electron counting scheme for $Ni_6(C_5H_5)_6$ attributed 90 electrons to metal–metal and metal–ligand bonding. The polyhedral skeleton electron pair theory would predict a square antiprismatic structure [95–97]. Unfortunately, the structure shows the Ni_6 core to be octahedral as for 86 electron clusters like $Rh_6(CO)_{16}$ [100]. Steric constraints have been invoked to explain this behavior.

Wei and Dahl have used the LCAO–MO method for hexanuclear clusters such as $Co_6(\mu_3\text{-}S)(\mu_3\text{-}SC_2H_5)_3(\mu\text{-}SC_2H_5)(\mu\text{-}CO)_5(CO)_6$ [270]. This complex consists of two Co_3 triangles bridged by three μ_3-SC_2H_5 ligands. The ground state of each triangle is $a_1^2a_1^2e^4e^4e^{*4}a^{*2}_1$. If one assumes that the antibonding orbitals exactly cancel the effect of the corresponding bonding orbitals, then there are six electrons available to form metal–metal bonds. This was interpreted as there being three σ bonds within each triangle, but no metal–metal bonds between the triangular moieties [270].

(vii) Higher nuclearity cluster complexes

Mingos has performed an EHMO calculation on a molecular cluster with more than six metal atoms. His studies dealt with the gold clusters $Au_9L_8^{3+}$, $Au_8L_8^{2+}$, and $Au_{11}L_7^{3+}$, where L is a phosphorus donor ligand [271]. The metal core was treated first and the ligand effects were included as perturbations upon the central electronic structure. The 6*s* orbitals were found to be important in the metal–metal bonding scheme, and both radial and peripheral bonding was important in these clusters, which have a single metal atom at the center. This finding was contrary to previous reports which emphasized one or the other of these two effects [272–276]. The gold clusters were found not to adhere to the established electron counting rules and factors which contribute to the breakdown were discussed.

C. SPECTROSCOPIC STUDIES

(i) Photoelectron spectroscopy

Photoelectron spectroscopy has recently become an important technique for investigating the electronic structure of inorganic complexes. Reviews on both ultraviolet photoelectron spectroscopy (PES) [67] and X-ray photoelectron phenomena (XPS) [71,277,278] have appeared. The ability to study chemisorbed substrates as well as molecular species by photoelectron spectroscopy has allowed a direct comparison of ligand binding in clusters and on metal surfaces. The XPS spectra of carbon monoxide in transition metal carbonyl compounds and CO absorbed onto the corresponding metal surface show remarkable similarities [272]. Even the mononuclear carbonyls exhibit nearly all the features of metal-adsorbed CO. Clusters of three or four metal atoms were found to adequately reproduce the spectrum of CO on a surface [277]. The shake-up energies as well as the oxygen 1*s* binding energies were used to evaluate CO binding. Analysis of the XPS spectrum of $Co_4(CO)_{12}$ reveals that bridging carbonyls back bond to a greater extent than do the terminal carbonyls [279]. X-ray photoemission techniques were applied to $Ir_4(CO)_{12}$ adsorbed onto a gold crystal [280]. Electron energy loss and Auger data were compared to previous XPS and ultraviolet visible studies, and analogies to CO on iridium were noted. A description of the metal–metal bonding in the oligomers of $[Pt_3(CO)_6]_n^{2-}$ ($n = 2, 3, 4, 5, 6, \sim 10$) by XPS showed very little interaction between trinuclear units [281]. Each Pt atom was assigned a $5d^{10}$ configuration, with the observed signal from these valence electrons split by 1.3 eV in all cases. This behavior was ascribed to spin-orbit coupling, with a value comparable to that of a free 5*d* electron. The binding energies of the 4*f* and 4*d* levels were found to have a $1/n^2$

dependence, indicating charge delocalization throughout the cluster.

The XPS technique has also been used to probe structural features. The $2p_{3/2}$ iron XPS signal from $HFe_3(CO)_{11}^-$ confirmed the presence of a unique iron atom in the cluster [282], a feature seen in earlier Mossbauer and X-ray structural analyses [283,284].

Walton and co-workers have published the XPS spectra of a number of $Re_3X_9 \cdot 3L$ and $Mo_6X_8^{4-}$ compounds (X = Cl, Br; L = N, P, O donors) [278,285–287]. Variation of the donor ability of L does not greatly affect the Re_3X_9 bonding. Ultraviolet photoelectron spectra have been reported for Re_3Cl_9 [205,206] and Re_3Br_9 [206]. These measurements in conjunction with theoretical calculations helped delineate the nature of metal–metal and metal–ligand bonding in these compounds (see Section B). A platinum halide cluster compound has been studied and its XPS spectrum compared to that of the bulk metal [288]. The results indicated strong metal–metal bonding in Pt_6Cl_{12}.

Large gold clusters have been of interest because the structures contain a central gold atom encased in a gold polyhedron [271,289,290]. The XPS spectra of $Au_{11}L_7^{2+}$, $Au_9L_8^{3+}$, and $Au_8L_8^{2+}$ (L = PR_3; R = Aryl group) are very similar and show the central atom to be distinct from its neighbors. The central gold has much less electron density than the other gold atoms, and consequently possesses a lower binding energy (ca. 6 eV difference). The studies further evidence strong electron delocalization throughout the cluster [289].

A variety of spectroscopic techniques, including XPS, were used to characterize $Fe_4S_4(SCH_2C_6H_5)_4^{2-}$, a model for ferrodoxin and high potential iron proteins [291]. The iron atoms were shown to be equivalent, and the sulfur $2p$ binding energies similar to those in the biochemical systems. The same analysis was performed on another sulfur cluster $Mo_3S_{13}^{2-}$. The XPS showed the six S_2 units to be essentially S_2^{2-} and the molybdenum values consistent with the 4+ oxidation state [292]. The Mo $3d_{5/2}$ XPS signal from $(Mo_6Cl_8)Cl_4$, formally a Mo(II) compound, is essentially the same (230.2 eV) as found in Mo(IV) complexes such as MoS_2, MoO_2, and $Mo_3S_{13}^{2-}$ [259]. This deviation was attributed to non-uniform charge distribution in the cluster. Broadening of all the XPS signals was assigned to this same strange phenomenon.

Vapor phase ultraviolet photoelectron spectra have been reported for a number of metal cluster carbonyl compounds. This technique is useful for directly probing the energies of the valence d electrons as they are well separated and to lower energy than the ionizations due to CO orbitals (see Fig. 9). The d electrons ionize between 7 and 12 eV, whereas the ligand localized electrons are more tightly bound and generally appear above 14 eV. Both He(I) ($h\nu = 21.2$ eV) and He(II) ($h\nu = 40.8$ eV) excitation sources were

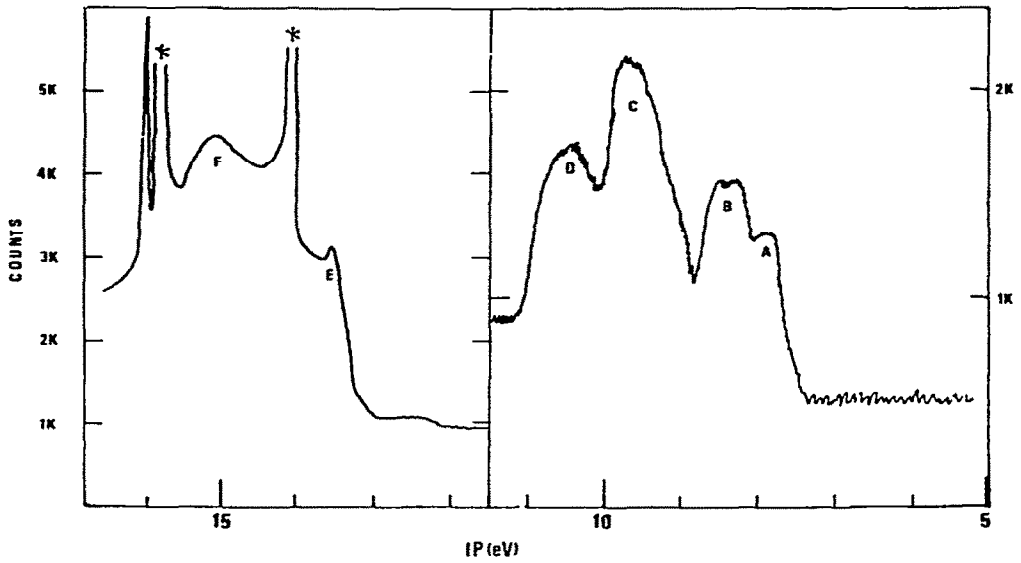

Fig. 9. Ultraviolet photoelectron spectrum of $Os_3(CO)_{12}$ with CO and Ar calibrants.

used to obtain spectra for $Ru_3(CO)_{12}$, $Os_3(CO)_{12}$, and $Os_6(CO)_{18}$ in the *d* band region (7–12 eV) [293]. Subsequently, the entire He(I) spectrum of $Ru_3(CO)_{12}$ was published along with a CNDO calculation to help assign the spectroscopic features [119] (see Section B). Photoelectron spectra of the hydrocarbonyls $H_3Re_3(CO)_{12}$, $H_4Os_4(CO)_{12}$, and $H_2Os_3(CO)_{10}$ were reported and interpreted in terms of a 3 center–2 electron bonding scheme, using a topological model similar to that used for boranes [294].

Condensed phase PES spectra are also known. The sample is usually adsorbed onto a pure metal crystal and the experiment is performed in a similar fashion as XPS. The spectrum of $Rh_6(CO)_{16}$ on copper is almost identical to that of CO on Pd(III) [295], again emphasizing the gross similarities in CO binding on surfaces and in metal complexes. The spectra of $Os_3(CO)_{12}$ and $Ir_4(CO)_{12}$ are similar to their XPS counterparts [277,280]. Triiron dodecarbonyl yields a PES spectrum that is similar to that of $Os_3(CO)_{12}$ [277].

(ii) Optical spectroscopy

Electronic transitions in transition metal cluster complexes usually occur in the visible and ultraviolet regions of the spectrum. Optical spectroscopy therefore allows direct characterization of the lowest unoccupied molecular orbitals [296].

Optical spectra of naked transition metal atoms and clusters have been thoroughly studied, and an extensive review has recently appeared [297]. Formation of these clusters has often been diagnosed by the growth of new broad electronic absorption bands, which contrast with the sharp atomic spectra. Cluster size is determined by monitoring the dilution and annealing dependence of electronic absorption bands. A theoretical model for clustering upon deposition has been developed [304]. Ozin and co-workers have introduced the technique of cryophotoclusterification, where selective irradiation leads to a $M_x + M \rightarrow M_{x+1}$ reaction [168,298–303]. The kinetics of this process have been determined for M = Ag [300].

Small silver clusters have received the most attention due to their importance in catalytic and photographic processes. Silver species as large as Ag_7 have been assigned and their corresponding band maxima noted [167,168]. The same clusters have been formed by the photoclusterification approach [298–300]. Welker and Martin have disputed these assignments based upon EHMO calculations and their own matrix isolation work [166]. In particular, for the following photoprocess the peak area of the band associated with the dimer

$$Ag + Ag_2 \rightarrow Ag_3$$

initially increases and suggests more complex behavior than simple, stepwise photoaggregation. The optical spectra of gold and nickel trimers have been reported, with some evidence for higher oligomers [305]. An extensive theoretical study of small nickel clusters has recently appeared and will greatly aid in the characterization of the electronic properties of these materials [159]. Copper species up to Cu_5 have been observed spectroscopically, and comparison of the optical spectra to that of the bulk shows little similarity [303, 306]. Selective photoaggregation techniques have also been used to obtain visible-ultraviolet spectra of Cr_3, Mo_3, Ag_2Cr, $CrMo_2$, and Cr_2Mo [168,301,302]. Small clusters have been supported on polymers by a metal vapor technique: Discrete Mo_5 and Cr_3 species have been observed [307].

Matrix isolation methods can also be applied to reactions of small metal clusters with ligands, to form species that would be quite unstable under ambient conditions. Hanlan and Ozin have made $Rh_3(O_2)_m$ ($m = 2$ or 6) and recorded its UV-VIS spectrum [308]. Reactions of this type with single atoms or diatomics are already well known [297].

The rhenium(III) halide trimers, Re_3X_9 (X = Cl, Br), were the subject of many early investigations. Their optical spectra under a variety of conditions have been reported [309–314]. The spectrum of $Cs_3Re_3Cl_{12}$ (Figs. 10 and 11) is typical of the spectra of these complexes. Intense bands are found at 515 nm (ϵ = ca. 1600) and 350–300 nm. These two features are assigned [312] to

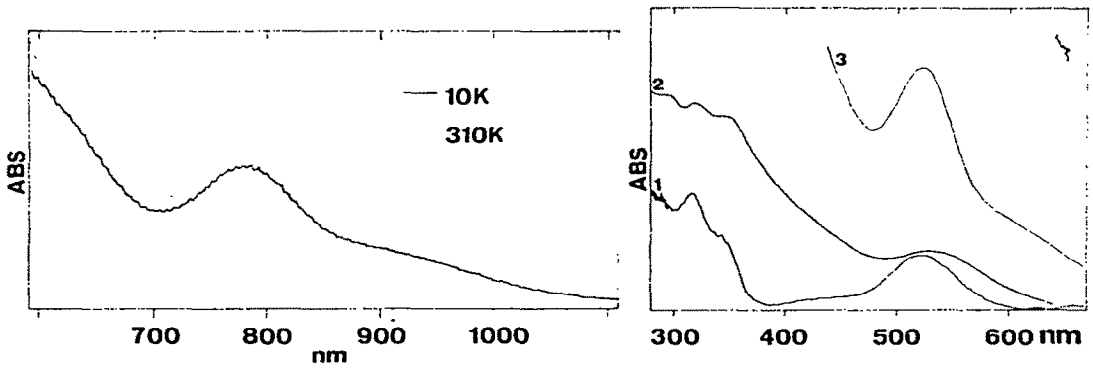

Fig. 10. Optical spectrum of $Cs_3Re_3Cl_{12}$ in the near IR region.

Fig. 11. Optical spectra of $Cs_3Re_3Cl_{12}$: (1) crystal spectrum; (2) spectrum in KCl pellet at 10 K; (3) spectrum in CsI pellet at 10 K.

metal–metal $\pi \rightarrow \pi^*$ and chloride to metal charge transfer transitions respectively. The weak (ϵ = ca. 400) absorption band system at 750 nm appears to consist of two components and the temperature dependence would indicate an allowed electronic transition. This band system has been attributed to metal localized $\pi \rightarrow \pi^*$ and $\pi \rightarrow \sigma^*$ one electron excitations. A very weak peak at 1200 nm has been attributed to the HOMO $\rightarrow$ LUMO transition; however, the large spin orbit coupling of Re might complicate the simple interpretation. Attempts to measure the electronic spectrum of $Re_3Cl_{12}^{3-}$ in a molten salt medium showed only decomposition to $Re_2Cl_8^{2-}$ and rhenium metal [313]. The electronic spectrum of Re_4Br_{15}, another compound containing the trinuclear rhenium cluster, was found to be similar to Re_3Br_9, but no assignments were offered [315].

Electronic spectra have been recorded for the hexanuclear halide clusters of molybdenum ($Mo_6X_8^{4+}$), niobium, and tantalum ($M_6X_{12}^{2+}$). Sheldon has reported two bands at 308 and 345 nm in the spectra of $Mo_6Cl_8^{4+}$ salts in 5 M HCl [316,317], designating them as charge transfer bands of unknown origin. Although the spectra of the hexameric niobium and tantalum halides, $M_6X_{12}^{2+}$, have appeared numerous times [64,318–323], few attempts have been made to assign them. Robin and Kuebler's MO calculation attributed the main features of the optical spectrum of $Nb_6Cl_{12}^{n+}$ ($n = 2, 3, 4$) [64] to *d–d* transitions and symmetry-forbidden charge transfer bands. A detailed summary of early theoretical work on $M_6X_{12}^{2+}$ clusters as well as explicit assignments for the optical transitions have been presented [318]. The low energy bands ($< 20\,kK\ cm^{-1}$) have been ascribed to five metal localized transitions. Bands occurring in the ultraviolet region were thought to be of a

charge transfer variety. Other contemporary work reported spectral data, but offered no specific assignments [319,320,322]. Espenson and McCarley were the first to report the spectra of $Ta_6Cl_{12}^{n+}$ ($n = 2, 3, 4$) [322]. The higher oxidation states were achieved by reaction with Fe^{3+}, and kinetic data were taken. Application of magnetic circular dichroism spectroscopy (MCD) to this problem allowed further characterization of the optical spectrum [321]. These measurements, along with EPR [324] and magnetic susceptibility studies [325], gave a ground state configuration of $a_{1g}^2 t_{1u}^6 t_{1u}^6 a_{2u}^2$. The two lowest unoccupied orbitals were t_{2g} in symmetry. The bands below 30000 cm^{-1} were assigned to metal localized transitions involving the orbitals mentioned above. At higher energy, LMCT transitions occurred [321].

The optical spectra of other niobium and tantalum halide clusters have been reported. Hexamethylbenzene complexes of the trinuclear and hexanuclear complexes have similar spectra [326]. The visible–near IR region of the spectrum has been recorded for Nb_3X_8 and $Nb_4X_{11}^-$ (X = Cl, Br) [323]. No assignments for either have been suggested.

The $(\eta^5\text{-}C_5H_5)_4Fe_4(CO)_4^n$ complexes are known to exist for $n = -1$ to $n = +2$. Spectra are known for all species except the dication [327,328]. Bock and Wrighton have identified a charge transfer to solvent band in the neutral compound, the intensity of which is linearly related to the Korower Z values [329,330]. This charge transfer band may explain the photooxidation observed in halocarbon solvents [328]. The optical spectra of iron carbonylmetallates and carbonylhydrides such as $HFe_3(CO)_{11}^-$, $Fe_3(CO)_{11}^{2-}$, $HFe_4(CO)_{13}^-$, and $Fe_4(CO)_{13}^{2-}$ have been known for quite some time [331,332], but no rigorous assignments have been proposed. Neutral carbonyl clusters have received more attention. Spectra for $M_3(CO)_{12}$ (M = Fe, Ru and Os) and $M_4(CO)_{12}$ (M = Co, Rh and Ir) are well known [208,213,331,333–335]. Chini and co-workers have even examined all the known mixed metal clusters of the $M_4(CO)_{12}$ series [334,335].

A large amount of theoretical work has concerned the trinuclear carbonyls [119,211,213,214] (see Figs. 3 and 4). This has lent invaluable assistance to the task of characterizing their optical spectra. Although qualitative assignments for metal localized transitions had already been made [333,334], it was not until the EHMO study of Tyler et al. that specific states were identified [213]. Their work was also aided by MCD studies [213] to detect E' excited states (see Section B). The iron analog, $Fe_3(CO)_{12}$ poses another problem. It possesses bridging carbonyl groups and its spectrum is more complicated [208,213,333]. Whether the "extra" transitions are due to charge transfer to the bridging carbonyls as previously suggested [208], or to splitting caused by the lower symmetry of the molecule is uncertain [213]. Recently, the optical spectrum of $HOs_3(CO)_{12}^+$ has been obtained and assigned [214].

The spectra of mixed metal carbonyl clusters are not only known for the

$M_4(CO)_{12}$ series (M = Co, Rh, Ir) and the $M_3(CO)_{12}$ compounds (M = Fe, Ru, Os) [333–335], but the mixed iron–Group VII metal carbonyls have also been characterized by optical spectroscopy [211,333]. Spectra for the $MFe_2(CO)_{12}^-$ anions are known for all three metals in the family (M = Mn, Re, Tc) [333]. The linear trinuclear complexes $M_2Fe(CO)_{14}$ have a number of unexplained weak features [213] and the mixed metal clusters $CoM_3(CO)_{13}$ and $HCoM_3(CO)_{13}$ (formed by reaction of $Co(CO)_4^-$ and the closed shell $M_3(CO)_{12}$ complexes) each show an intense transition in the visible [336]. Optical spectra have also been measured for the mixed dihydrides $H_2FeRuM_3(CO)_{13}$ (M_2 = Ru_2, RuOs, Os_2) [333,337]. Analogies have been drawn between the visible spectra of $H_3M_3(CO)_{12}$ (M = Mn, Re) and the isoelectronic triiron and triosmium dodecarbonyls [338].

The Fe_4S_4 clusters have been of interest as models for bioinorganic systems. An extensive study [291] of $Fe_4S_4(SCH_2C_6H_5)_4^{2-}$, a model for ferrodoxin and high potential iron proteins, concluded that the optical spectrum (with bands at 290 and 390 nm) was similar to that of the naturally occurring systems [339,340]. These transitions appear to derive from delocalized states in the Fe_4S_4 core [291]. The methyl analog, $Fe_4S_4(SCH_3)_4^{2-}$ shows bands at 295 and 418 nm [237]. Aided by an SCF–Xα–SW calculation, these transitions were assigned to sulfur to iron charge transfer and a weak band at 650 nm assigned to a *d–d* transition. Müller and co-workers have investigated Mo–S complexes and recently reported the UV–VIS spectrum of $Mo_3S_{13}^{2-}$ [287]. The lowest energy band was assigned to *d–d* transitions in the Mo_3 moiety. To higher energy, a charge transfer band of the type $\pi^*(S_2^{2-}) \rightarrow \sigma^*(d_{Mo})$ occurred. The optical spectrum of a reduced tetrathiometallate complex, $[(MoS_4)_2Fe]^{3-}$, has also been reported, but no specific assignments were possible [341].

A novel bent trinuclear cluster $\{Cu(dien)\}_2Fe(CN)_6 \cdot 6H_2O$ has been prepared [342]. Although there are no formal metal–metal bonds, charge transfer bands assigned to $Fe^{2+} \rightarrow Cu^{2+}$ have been identified. Three intense bands are observed in the visible spectral region for $Cp_3Ni_3(\mu_3\text{-}NC(CH_3)_3)$, a cluster containing a triply bridging nitrene functionality [343]. Optical spectra for salts of $Pd_3(PPh_3)_3(\mu_2\text{-}PPh_2)_3^+$ have also been reported [232].

(iii) Electron paramagnetic resonance spectroscopy

The technique of electron paramagnetic resonance (EPR) spectroscopy is invaluable in the characterization of metal cluster complexes having unpaired electrons. Spectra have been reported for naked metal clusters as well as for molecular complexes. Using the theory introduced by Fröhlich [25] and elaborated by others [344,345], Kubo [24] and Kawataba [165] have shown that the bandwidth and g-shift of the EPR signal of a small metallic

cluster of silver is directly related to the size of the microcrystal. The dimensions of these silver clusters trapped in rare gas matrices were estimated at ca. 10 Å in diameter, roughly corresponding to a face centered cubic Ag_{13} species [346]. A hexanuclear Ag^I cluster $[Ag(imid)]_6(ClO_4)_6$ also yields an EPR signal [347]. Mixed Ag^I/Ag^0 clusters have been prepared in zeolites and there appears to be both Ag^I-Ag^I and Ag^0-Ag^0 metal–metal bonding [348,349]. Disagreement has risen over the actuality of bonding between silver(I) ions [350,351]. It appears from recent examples that there is at least a weak interaction [352,353].

The niobium halide cluster $Nb_6Cl_{12}^{3+}$ yields a signal at $g = 1.95$ with ^{93}Nb fine structure [324]. This indicates electron delocalization throughout the metal cluster framework. In the trimeric niobium cluster $[Nb_3Cl_6(C_6Me_6)_3]^{2+}$ there is also one unpaired electron that is metal centered [354]. The EPR signal is broad with a nearly isotropic g value ($g = 1.996$). Conductivity measurements indicate semiconductor behavior with a room temperature conductivity of 1×10^{-3} ohm^{-1} cm^{-1}, suggesting that some mechanism for electron exchange between clusters must exist.

The hexanuclear species, $Mo_6Cl_8^{3+}$ and $Mo_6Cl_8^{5+}$, generated in a glass by γ irradiation are EPR active [355]. The oxidized species has a highly anisotropic g value ($g = 1.933$, $g = 2.122$), indicative of a degenerate HOMO. This is assigned as the metal localized t_{2u} orbital. The reduced species, on the other hand, has an isotropic g value ($g = 1.943$), assigned to an electron residing in the antibonding a_{2g} orbital. Support for a non-degenerate orbital occupation in this case is given by $Mo_6Cl_8^{2+}$, which is diamagnetic. The measurements also determined the relative ordering of the d orbitals [355].

The $Co_3(CO)_9S$ complex contains one unpaired electron, and has been subjected to an EPR analysis [225,226]. On the basis of this work, the electron has been assigned to an a_2 orbital which is primarily of d character. This antibonding orbital is localized in the Co_3 plane. As a result, the Co–Co bond lengths are significantly longer (2.64 Å) than in the corresponding diamagnetic cluster $FeCo_2(CO)_9S$ (2.55 Å) [226]. Similar results were obtained for $Co_3(CO)_9Se$. Hyperfine coupling due to the ^{59}Co nucleus ($I = 7/2$) has only been detected in single crystal studies [226]. All twenty-two lines could be resolved upon excitation perpendicular to the three-fold axis. The g value observed for the isoelectronic $Co_3(CO)_9CR^-$ species was almost identical and an analogous assignment for the HOMO symmetry (a_2) can be made [356] (R = Cl, $g = 2.020$). Isoelectronic nickel clusters $Cp_3Ni_3(\mu_3\text{-}(CO)_2)_2$ and $Cp_3Ni_3(\mu_3\text{-}NC(CH_3)_3)$ have also been prepared. The latter compound shows no ^{14}N hyperfine coupling from the bridging nitrene moiety, which suggests that the unpaired electron is metal localized [343]. The orbital was described as π-bonding between metal atoms, in agreement with the studies on the tricobalt systems. The structure shows slight distor-

tion from three-fold symmetry with Ni–Ni bond lengths of 2.39, 2.37 and 2.34 Å. This was attributed to Jahn–Teller effects or possibly crystal interactions; however, the distortions seem too large for the latter. The original work on $Cp_3Ni_3(CO)_2$ assigned the unpaired electron to a metal–metal bonding orbital [357]. This was later shown to be incorrect, as its bond lengths are longer than the diamagnetic analogue $Cp_3CoNi_2(CO)_2$ [226]. The g shifts and bandwidths are not inconsistent with an assignment similar to those mentioned aforehand [357].

A large number of metal carbonyl clusters have been irradiated in glasses to produce the radical anions. The spectra have been communicated, but no extensive analysis concerning the significance of the data or identity of the EPR active species has appeared [358,359]. Of particular note are the signals obtained for the trinuclear carbonyls $Fe_3(CO)_{12}$ ($g = 2.051, 2.003$), $Ru_3(CO)_{12}$ ($g = 1.982$), and $Os_3(CO)_{12}$ ($g = 2.001$). It was later shown that the radical anions of $Ru_3(CO)_{12}$ and $Os_3(CO)_{12}$ decomposed readily to give unidentifiable products [360]! The radical anion of $Fe_3(CO)_{12}$ appears to be stable at low temperatures and the reduction is completely reversible [359,360]. The g value is reported as 2.004, and warming leads to a decomposition product with two signals at $g = 2.05$ and 2.00 [359].

The $[Fe_4Mo_4S_{20}]^{6-}$ cluster [361], later shown by X-ray crystal structure analysis to be $[(MoS_4)_2Fe]^{3-}$ [341], has three unpaired electrons ($\chi = 3.85\ \mu_B$). The EPR spectrum exhibits resonances at $g = 4.6$, 3.3, and 2.0 [362].

(iv) Magnetic susceptibility measurements

The hexameric $Ni_6(C_5H_5)_6$ contains two unpaired electrons and its monocation three [100]. It was concluded that the HOMO is triply degenerate in this molecule of O_h symmetry. The ground state is assigned as $^4A_{2u}$ for the monocation, presuming the HOMO to be the metal–metal antibonding t_{2u} orbital. This predicts a $^3T_{1g}$ ground state for the neutral species. Other nickel clusters with unpaired electrons are known. The tetranickel cluster hydride $Cp_4Ni_4H_3$ has three unpaired electrons as determined by bulk magnetic measurements [243]. No convincing explanation was given; however, accidental degeneracy was proposed. Subsequent analysis by Hoffmann et al. placed three electrons in a nearly triply degenerate metal-centered orbital of t_1 pseudosymmetry (see Section B). The $Cp_3Ni_3(\mu_3\text{-}NC(CH_3)_3)$ molecule with a triply bridging nitrene group shows one unpaired electron ($\chi = 3.85\ \mu_B$ at 300 K). The tetranuclear iron–sulfur cluster $Fe_4S_4(\eta^5\text{-}C_5H_5)_4^+$ has had its magnetic susceptibility measured numerous times [234,344,363,364], giving values of 0.96–1.33 μ_B. The neutral $Cp_4Fe_4S_4$ is diamagnetic, but has a temperature independent paramagnetism (TIP) of 0.80 μ_B. The

$Fe_4S_4(SCH_2C_6H_5)_4^{2-}$ cluster, with a μ_{eff} of 1.04 μ_B [291], has a magnetic moment similar to the biological system it models [365].

Magnetic susceptibility measurements on the $Mo_6X_8^{4+}$ (X = Cl, Br) clusters indicate they are diamagnetic [258–263,317] in accord with the many theoretical schemes proposed for these compounds. The analogous $Nb_6X_{12}^{2+}$ systems are also diamagnetic, but with a large TIP [324]. The oxidized species $Nb_6Cl_{12}^{3+}$ has a magnetic moment of 1.62 μ_B corresponding to one unpaired electron, consistent with other spectroscopic data including the EPR data ($g = 1.95$) [324].

(b) Electrochemistry

The electrochemical reduction of a transition metal cluster complex frequently results in concomitant metal–metal bond cleavage as often found for dinuclear species such as $Mn_2(CO)_{10}$ [366]. As opposed to dimers the additional charge and bond ordering can be delocalized throughout a larger cluster's metal core. Consequently, some species undergo many reversible electrochemical cycles without declusterification. The hexameric $Ni_6Cp_6^n$ complex can exist with n varying from -1 to $+3$ [100]. Since the four highest energy electrons occupy metal–metal antibonding orbitals, their removal by electrochemical oxidation is quite facile (see diagram below). The voltages are measured versus a standard calomel electrode (SCE).

$$Ni_6Cp_6^- \xrightarrow{-0.97\ V} Ni_6Cp_6 \xrightarrow{-0.26\ V} Ni_6Cp_6^+ \xrightarrow{+0.19\ V} Ni_6Cp_6^{2+} \xrightarrow{+1.0\ V} Ni_6Cp_6^{3+}$$

The $Cp_4Fe_4S_4$ cluster can be oxidized through the series from monoanion to trication [235] (see below). The voltages listed are uncorrected junction potentials at a platinum electrode.

$$Fe_4S_4^- \xrightarrow{-0.33\ V} Fe_4S_4 \xrightarrow{+0.33\ V} Fe_4S_4^+ \xrightarrow{+0.88\ V} Fe_4S_4^{2+} \xrightarrow{+1.41\ V} Fe_4S_4^{3+}$$

$Fe_4S_4 = Cp_4Fe_4S_4$

The niobium chloride cluster, $Nb_6Cl_{12}^{2+}$, can be doubly oxidized and each of the resultant clusters are stable and have been isolated [190]. The first oxidation occurs at -0.10 V (vs. SCE) and the second at $+0.70$ V (vs. SCE). The niobium and tantalum clusters with bound hexamethylbenzene ligands, $M_3Cl_6(C_6Me_6)_3^{2+}$ (M = Nb, Ta), can be oxidized or reduced. The processes, using a silver/silver(I) chloride couple, occur at ca. -0.2 V for the oxidation and ca. -2.0 V for the reduction [194].

Using the same couple, the tricobalt carbon clusters, $Co_3(CO)_9CR$, reversibly reduce to the radical anion. The potential varies with the organic substituent R [367]. Cyclic voltammograms were given for a number of these compounds. Triiron dodecacarbonyl, well known to undergo one electron reduction to the radical anion [216,241–243], has been reported to undergo a

second reversible reduction to $Fe_3(CO)_{12}^{2-}$ [241,243]. Potentials for the two steps are −0.44 and −0.83 V vs. SCE, respectively. The same reduction has been carried out using the Ag/AgCl couple [243]. The one-electron reduction potentials for a number of the phosphine substituted derivatives of $Fe_3(CO)_{12}$ have also been measured. With only one exception, they cannot be cleanly oxidized [243]. The $Fe(CO)_9(P(OMe)_3)_3$ cluster reversibly oxidizes to the radical cation. Employing a dropping mercury electrode and low temperatures, the carbonyl hydride species $HFe_3(CO)_{11}^-$ can be reversibly reduced. The triruthenium- and triosmiumdodecacarbonyls decompose upon reduction [243], contrary to previous reports [216]. A number of other carbonyl cluster compounds have had their one electron reduction potentials measured [242]. The tetrameric $Fe_4S_4(SCH_2C_6H_5)_4^{2-}$ compound, similar to the $Cp_4Fe_4S_4$ cluster above may be reduced reversibly, but will oxidize irreversibly at a dropping mercury electrode [162]. Attempts to use a platinum electrode did not succeed because of cluster adsorption to the surface. Other sulfur clusters such as $Fe(MoS_4)_2^{3-}$ [362] and $Mo_3S_{13}^{2-}$ [103] have been studied by cyclic voltammetry.

(vi) Resonance Raman spectroscopy

As the excitation frequency in a Raman experiment approaches an electronic transition, an intensity enhancement occurs for those normal modes distinctly coupled to the resonant state [367–371]. For an electric dipole allowed transition, the totally symmetric modes will be those primarily enhanced. The magnitude of the effect will depend on (1) the frequency difference between the excitation line and the resonant state's energy, (2) the Franck–Condon overlap factors, and (3) the intensity of the electronic transition. In addition to an increase in the intensity of the fundamental, a number of overtone and combination bands may be observed. If the excited state is degenerate, Jahn–Teller active modes, which appear to be totally symmetric in the distorted excited state, may be enhanced [371]. In the case of vibronically allowed, electric dipole forbidden transitions, the vibronically enabling modes may be enhanced, but the effect is usually small due to the lesser intensities of these types of bands. Interference effects and resonance deenhancements are also possible in dipole forbidden transitions.

The resonance Raman spectrum of Re_3Cl_9 in the solid state and isolated in an argon matrix has been investigated [372]. The totally symmetric Re_3 breathing mode shows a dramatic increase in intensity and three overtones appear upon excitation into the first intense band. In the matrix, the totally symmetric mode appears at 277 cm^{-1} compared to 250 cm^{-1} in the solid. In addition, numerous combination bands, which involve an out-of-plane Re–

TABLE 5

Wavelength dependence of intensities of Raman active metal–metal stretching modes in $Co_4(CO)_{12}$ [a]

Wavelength (Å)	247 cm^{-1}	183 cm^{-1}
6471	1.0	1.0
5145	1.1	4.4
4965	1.4	7.0
4880	1.6	7.2
4579	2.9	7.3
4545	4.6	7.4

[a] Values denoted are relative to initial intensity at 6471 Å.

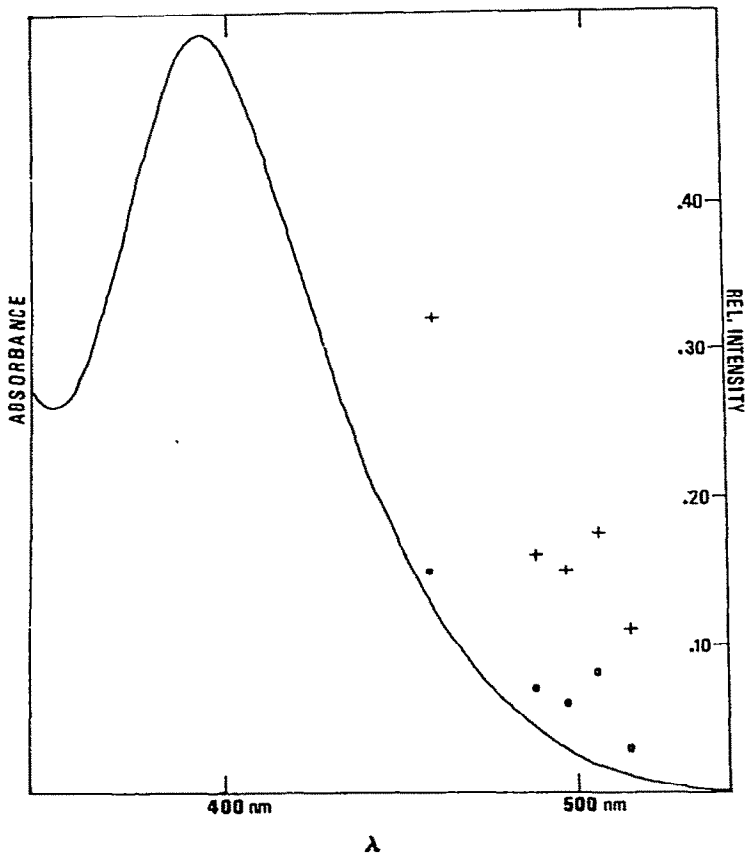

Fig. 12. Excitation profile and electronic absorption spectrum of $Ru_3(CO)_{12}$: (+), totally symmetric metal–metal stretching mode, a_1'; (○), non-totally symmetric metal–metal stretching mode, e'.

Re deformation (72 cm^{-1}), appear in the matrix spectrum.

Resonance enhancement has been observed for the metal–metal stretches in $Co_4(CO)_{12}$ [373,374]. Totally symmetric modes are observed at 247 and 183 cm^{-1}, corresponding to the metal–metal bonds with and without carbonyl bridges, respectively [374]. The excitation profile confirms the presence of a weak band at 4800 Å, and that the band at 3750 Å is of metal–metal bonding to antibonding character [214] (see Table 5). The excitation profile of $Ru_3(CO)_{12}$ reveals that both the totally symmetric and e' M_3 modes exhibit resonance enhancement (see Fig. 12) [214]. As the excited state is degenerate, the e' vibration is Jahn–Teller active and signals a distortion of the metal framework in the excited state [214]. Such behavior may dictate the photofragmentation often observed with $Ru_3(CO)_{12}$ [375,376]. The symmetric metal–metal stretch in $Cp_4(CO)_4$ also shows a resonance enhancement upon excitation into the lowest energy electronic absorption band [377(a)]. This band at 540 nm is predicted to be metal localized (see Section B).

Resonance Raman spectra of matrix isolated Ni_3 shows it to be bent with a bond angle of ca. 100° [377(b)]. Up to six overtones of the totally symmetric stretch (232 cm^{-1}) were observed. The ground state was assigned as Δ_u in symmetry, and evidence for Renner–Teller distortion was given.

(vii) Mössbauer spectroscopy

The Mössbauer effect arises from the absorption of γ-radiation by a radioactive nucleus. Nuclear transitions are chiefly influenced by the orbitals showing the greatest nuclear penetration, i.e. the *s* electrons. Therefore, the isomer shift, or energy of this transition, directly reflects the electron density. In addition, if the nucleus possesses a non-integral spin and is in a non-cubic symmetry environment, quadrupole splittings may arise.

Of all the nuclei of cluster forming metals, ^{57}Fe is the most conducive to this type of spectroscopy. As a result, almost all studies on metallic cluster compounds involve iron. Greenwood and co-workers were the first to report the Mössbauer spectra of some metal cluster complexes and studied the common iron carbonyls, carbonyl metallates, and carbonyl hydrides [283,378]. They also measured the spectra of $Fe_4Cp_4(CO)_4$ and its monocation [378]. The latter two compounds possessed identical isomer shifts and only one type of iron was seen in both compounds. This indicates the HOMO is delocalized over all the iron atoms or perhaps that it is not involved in metal–metal bonding. Theoretical studies have shown this orbital to be metal–metal non-bonding [234] (see Section B). The Mössbauer spectrum of $Fe_4S_4(SCH_2C_6H_5)_4^{2-}$ shows all the iron atoms to be in equivalent environments [291], but the isomer shift and quadrupole splitting do not

agree with the biochemical systems this compound is supposed to model [379–381].

The only other data available on iron clusters are for mixed iron–cobalt and iron–rhodium carbonyl clusters [382,383]. Substitution of $HFeCo_3(CO)_{12}$ with phosphorus donor ligands did not seem to affect the isomer shift [383]. Mössbauer spectroscopy was used to show that $CpCoFe_2(CO)_9$ and $CpRhFe_2(CO)_9$ are not isostructural [382].

The ^{197}Au Mössbauer spectrum of $Au_{11}L_7X_3$ ($L = Pr_3$; $X = Cl$) compounds verify that the central gold atom has a different charge density and electronic structure than the peripheral relatives [384]. Those outer atoms also exhibit differing shifts which depend upon coordination to chloride or phosphine. Only small interactions were evident between peripheral gold atoms.

D. PHOTOCHEMICAL STUDIES

Metal carbonyl cluster complexes and their derivatives provide compounds of photochemical interest. Recall that these species exhibit low energy electronic transitions to metal–metal antibonding excited states. Primarily two types of reactions are observed; (1) cleavage of metal–metal bonds and fragmentation to produce species of low nuclearity; (2) ligand (CO) substitution. The relative contributions of these processes are not very clear at the present time. Most investigations have been chiefly aimed toward synthesis and catalysis, and irradiation conditions have not been carefully specified. One tentative observation is that ligand substitution becomes more important for the third row metal complexes, presumably due to the increased strength of metal–metal bonding. The recent use of excited state vs. ground state electron density difference maps offers the possibility of visualizing the bonding properties in excited states [214].

Most cluster photochemistry has concerned the trinuclear $M_3(CO)_{12}$ (M = Fe, Ru, Os) compounds. Knox and Stone reported a number of reactions of $Ru_3(CO)_{12}$ and $Os_3(CO)_{12}$ with silanes, stannanes and germanes during ultraviolet photolysis [385–388]. The products were mostly mononuclear and of the type $(Me_3E)M(CO)_4H$ or $(Me_3E)_2M(CO)_4$ (M = Os, Ru; E = Sn, Si, Ge). Disilanes, on the other hand, exclusively yield [388] bridged dimers (1).

$$(Me_3Si)M(CO)_3(\mu_2\text{-}SiMe_2)_2M(CO)_3(SiMe_3) \qquad (1)$$

M = Os, Ru

Photolysis of $M_3(CO)_{12}$ in the presence of donor molecules and CO leads to the mononuclear species $M(CO)_4L$ ($L = C_2H_4$, PR_3; M = Fe, Ru, Os) [389]. Irradiation of $Os_3(CO)_{12}$ in the presence of the bidentate cyclooctadiene (COD) ligand also yields a mononuclear complex, $Os(CO)_3(COD)$ [390].

Tyler et al. [391] examined the photochemical reaction of $Os_3(CO)_{12}$ with chlorocarbon solvents. Although $Os(CO)_4Cl_2$ was the ultimate product, they presented some evidence for an $Os_3(CO)_{12}Cl_2$ intermediate. Burkhardt and Geoffroy [376] discovered that $[Co(CO)_4]^-$ photochemically adds to $Os_3(CO)_{12}$ to yield $[CoOs_3(CO)_{13}]^-$. Cullen et al. found that $M_3(CO)_{12}$ (M = Fe, Ru) photochemically reacts with bridging phosphines and arsines to yield trinuclear compounds $M_3(CO)_{10}$ (L–L) (L–L = $(Me_2As)C=C(AsMe_2)CF_2CF_2$, $(Ph_2P)C=C(PPh_2)CF_2CF_2CF_2$) [392–394]. Roberts and Trotter isolated the iron–phosphine compound and verified its nuclearity by X-ray structural analysis [395].

The ability of the $M_3(CO)_{12}$ clusters to catalytically isomerize olefins during irradiation has been studied by several groups [375,396–399]. The photogenerated species were also found to induce hydrosilation [375]. Larger metal hydrido clusters, such as $H_4Ru_4(CO)_{12}$, catalytically isomerize pentenes and stoichiometrically reduce them. Catalytic hydrogenation can be accomplished in the presence of 10 psi H_2 [400].

Transition metal hydrido carbonyl clusters such as $H_4Ru_4(CO)_{12}$ have accounted for some recent interesting results. The photolysis of $H_4Os_4(CO)_{12}$ with olefins (H_2C_2HR) has led to stable, isolable materials [401,402] of the form $H_3Os_4(CO)_{11}(HC_2HR)$. These complexes lose H_2 upon heating, but are otherwise very stable [402]. Trinuclear hydrides such as $H_3M_3(CO)_{12}$ (M = Mn, Re) yield cluster fragments as the major photochemical products [338]. The rhenium complex quantitatively produces $H_2Re_2(CO)_8$. Both trimers are known to isomerize pentenes upon photolysis [400]. These cluster complexes provide an interesting contrast to mononuclear hydrides, which frequently lose H_2 upon photolysis [403].

Geoffroy and Epstein have examined the declusterification of the methynyltricobalt cluster $HCCo_3(CO)_9$ [404]. Under H_2, CH_4 is produced and the cobalt fragment can be recovered as $Co_4(CO)_{12}$. Addition of CO during photolysis leads to $Co_2(CO)_8$ as the final product. Photolysis of $HFeCo_2(CO)_{12}$ also yields $Co_4(CO)_{12}$ as the ultimate cobalt cluster in the absence of added CO [403]. The photochemistry of larger carbonyl clusters is not well documented. Asinger et al. reported that irradiation of $Co_4(CO)_{12}$ with 1-undecene leads to olefin isomerization [397]. Photolysis of $Ir_4(CO)_{12}$ in the presence of $(MeCO_2)_2C_2$ gives the tetranuclear compound $[Ir_4(CO)_8\{(MeCO_2)_2C_2\}_4]$ in 35% yield [405].

A recent report has appeared on the photoreactivity of isocyanide bridged dirhodium cations, $Rh_2(br)_4^{2+}$ (br = 1,3-diisocyanopropane) [406]. The reaction scheme below outlines the results. Light induces redox chemistry as well as metal–metal bond cleavage in this novel system.

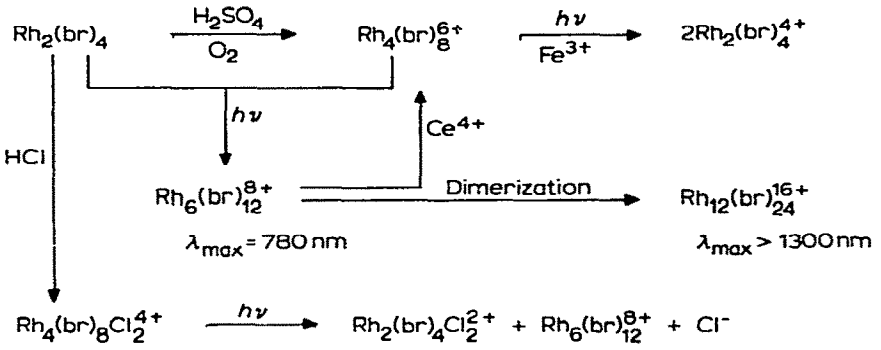

E. CONCLUDING REMARKS

It has probably been apparent that more experimental and theoretical work will be necessary before the electronic structure of metal cluster complexes can be regarded as a solved problem. Interesting questions posed by existing work include: (1) the relationship between electron counting rules and more quantitative theoretical models; (2) the energy barriers between several cluster or ligand geometries; (3) the strengths of the metal–metal bonds; (4) the extent of the similarity between metal surfaces, atomic clusters and metal cluster complexes; (5) the importance of metal valence *s* and *p* orbitals to metal–metal bonding; (6) the nature of bound H and CO in metal cluster complexes and its significance for Fischer–Tropsch chemistry; (7) the role the HOMO and LUMO play in redox reactions of cluster systems; (8) the relationship between excited state wavefunctions and photochemical reactivity.

ACKNOWLEDGEMENTS

We thank the Research Corporation and the Northwestern University Research Committee for support of our spectroscopic efforts. We thank Mrs. Carol Lewis for careful typing of the manuscript.

REFERENCES

1 F. L'Epiattinier, P. Matthys and F. Calderazzo, Inorg. Chem., 9 (1970) 342.
2 G. Pregaglia, A. Andreelta, G. Ferrari and R. Ugo, J. Organomet. Chem., 33 (1971) 73.
3 P. Pino, G. Braca, G. Sbrana and A. Cuccuru, Chem. Ind. (London), (1968) 1732.
4 R.P. Ferrari and G.A. Vaglio, Inorg. Chim. Acta, 20 (1976) 141.
5 M. Castiglioni, L. Milone, D. Osella, G.A. Vaglio and M. Valle, Inorg. Chem., 15 (1976) 394.

6 D. Bingham, B. Hudson, D.E. Webster and P.B. Wells, J. Chem. Soc., Dalton Trans., (1974) 1521.
7 L. Marko, in R. Ugo (Ed.), Aspects in Homogeneous Catalysis, Vol. II, Reidel, Holland, 1974.
8 P. Pino, F. Piacenti, M. Bianchi and L. Lazzaroni, Chim. Ind. (Milan), 50 (1968) 106.
9 G. Braca, G. Sbrana, F. Piacenti and P. Pino, Chim. Ind. (Milan), 52 (1970) 1091.
10 R.A. Sanchez-Delgado, J.S. Bradley and G. Wilkinson, J. Chem. Soc., Dalton Trans., (1976) 399.
11 R.M. Laine, R.G. Rinker and P.C. Ford, J. Am. Chem. Soc., 99 (1977) 252.
12 H. Kang, C.H. Maudlin, T. Cole, W. Slegeir, K. Cann and R. Pettit, J. Am. Chem. Soc., 99 (1977) 8323.
13 J. Falbe, J. Organomet. Chem., 94 (1975) 213.
14 G.A. Vaglio, D. Osella and M. Valle, Transition Met. Chem., 2 (1977) 94.
15 H.D. Kaesz, Chem. Br., 9 (1973) 344.
16 R. Ugo, Catal. Rev. Sci. Eng., 11 (1975) 225.
17 G.A. Ozin, Catal. Rev. Sci. Eng., 16 (1977) 191.
18 R.G. Wolley, Platinum Met. Rev., 24 (1980) 26.
19 E.L. Muetterties, Science, 196 (1977) 839.
20 E.L. Muetterties, Pure Appl. Chem., 52 (1980) 2061.
21 E.L. Muetterties, T.N. Rhodin, E. Band, C.F. Brucker and W.R. Pretzer, Chem. Rev., 79 (1979) 91.
22 J.C. Hemminger, E.L. Muetterties and G. Somorjai, J. Am. Chem. Soc., 101 (1979) 62.
23 M. Moskovits, Acc. Chem. Res., 12 (1979) 229.
24 R. Kubo, J. Phys. Soc. Jpn., 17 (1962) 975.
25 H. Fröhlich, Physica (Utrecht), 6 (1937) 406.
26 C. Ungerman, V. Landis, S.A. Moya, H. Cohen, H. Walker, R.G. Pearson and P.C. Ford, J. Am. Chem. Soc., 101 (1979) 5922 and references therein.
27 K. Kaneda, M. Hiraki, K. Sano, T. Imanaka and S. Teranishi, J. Mol. Catal., 9 (1980) 227.
28 R.L. Pruett and W.E. Walker, U.S. Pat., 3,957,857 (1976) and 3,898,214; 3,878,290; 3,878,292 (1975).
29 B.C. Gates and J. Lieto, Chem. Tech. (Leipzig), 19 (1980) 195.
30 J.H. Sinfelt, Prog. Solid State Chem., 10 (1977) 55.
31 D.L. Beach and T.P. Kobylinski, J. Chem. Soc., Chem. Commun., (1980) 933.
32 H. Alper and M. Gopal, J. Chem. Soc., Chem. Commun., (1980) 821.
33 H. Inoue and M. Suzuki, J. Chem. Soc., Chem. Commun., (1980) 817.
34 A.P. Humphries and H.D. Kaesz, Prog. Inorg. Chem., 25 (1979) 146.
35 A.K. Smith and J.M. Basset, J. Mol. Catal., 2 (1977) 229.
36 H. Vahrenkamp, Angew. Chem., Int. Ed. Engl., 17 (1978) 379.
37 Y. Sasaki, Kagaku No Ryoiki, 22 (1968) 906.
38 M.C. Baird, Prog. Inorg. Chem., 9 (1968) 1.
39 B.J. Bulkin and C.A. Rundell, Coord. Chem. Rev., 2 (1967) 371.
40 D.L. Kepert and K. Vrienge, Halogen Chem., 3 (1967) 1.
41 R.S. Nyholm, Adv. Sci., 23 (1967) 421.
42 H. Vahrenkamp, Chem. Unserer Zeit, 8 (1974) 112.
43 N.S. Voronovich, D.V. Korol'kov, K. Missner and V.N. Pak, V sb., Probl. Sovrem. Khim. Koordinats. Soedin., Leningrad, 1975, p. 208.
44 S. Otsuka, Shokubai, 10 (1968) 192.
45 J. Aihara, Bull. Chem. Soc. Jpn., 52 (1979) 2202.

46 G.R. John, B.F.G. Johnson and J. Lewis, J. Organomet. Chem., 181 (1979) 143.
47 C.E. Housecraft, K. Wade and B.C. Smith, J. Chem. Soc., Chem. Commun., (1978) 765.
48 J.M. Basset and R. Ugo, in R. Ugo (Ed.), Aspects in Homogeneous Catalysis, Vol. III, Reidel, Holland, 1977.
49 J. Lewis, Pure Appl. Chem., 10 (1965) 11.
50 (a) K. Wade, Chem. Br., 11 (1975) 177.
(b) K. Wade, Adv. Inorg. Chem. Radiochem., 18 (1976) 1.
51 K. Wade, J. Chem. Soc., Chem. Commun., (1972) 792.
52 D.M.P. Mingos, Nature (London), Phys. Sci., 236 (1972) 99.
53 K.M. Thomas, R. Mason and D.M.P. Mingos, J. Am. Chem. Soc., 95 (1973) 3802.
54 R. Mason and D.M.P. Mingos, MTP Int. Rev. Sci.: Phys. Chem., Ser. 2, 11 (1975).
55 R. Mason, K.M. Thomas and D.M.P. Mingos, J. Am. Chem. Soc., 95 (1973) 3802.
56 S.F.A. Kettle, J. Chem. Soc. A, (1967) 314.
57 S.F.A. Kettle, Theor. Chim. Acta, 3 (1965) 211.
58 S.F.A. Kettle, Theor. Chim. Acta, 3 (1965) 282.
59 S.F.A. Kettle, Theor. Chim. Acta, 4 (1966) 150.
60 S.F.A. Kettle, J. Chem. Soc. A, (1966) 1013.
61 S.F.A. Kettle and I.A. Khan, J. Organomet. Chem., 5 (1966) 588.
62 F.A. Cotton and T.E. Haas, Inorg. Chem., 3 (1964) 17.
63 J.E. Ferguson, B.R. Penfold, M. Elder and B.H. Robinson, J. Chem. Soc., (1965) 5500.
64 M.B. Robin and N.A. Kuebler, Inorg. Chem., 4 (1965) 978.
65 F.A. Cotton, Q. Rev. (London), 20 (1966) 389.
66 K.L. Watters and W.M. Risen, Inorg. Chim. Acta Rev., 3 (1969) 129.
67 A.H. Cowley, Prog. Inorg. Chem., 26 (1980) 45 and references therein.
68 W.C. Trogler, J. Chem. Educ., 57 (1980) 424.
69 J.L. Templeton, Prog. Inorg. Chem., 26 (1980) 211.
70 W.C. Trogler and H.B. Gray, Acc. Chem. Res., 11 (1978) 232.
71 R.A. Walton, Prog. Inorg. Chem., 16 (1972) 1.
72 S. Shaik, R. Hoffmann, C.R. Fisel and R.H. Summerville, J. Am. Chem. Soc., 102 (1980) 4555.
73 F.A. Cotton, Chem. Soc. Rev., 4 (1975) 27.
74 F.A. Cotton, J. Less-Common Met., 54 (1977) 3.
75 F.A. Cotton, Rev. Pure Appl. Chem., 17 (1967) 25.
76 F.A. Cotton, J.G. Norman, A. Spencer and G. Wilkinson, J. Chem. Soc., Chem. Commun., (1971) 967.
77 J.A. Baumann, S.T. Wilson, D.J. Salmon, P.L. Hood and T.J. Meyer, J. Am. Chem. Soc., 101 (1979) 2916.
78 J.A. Baumann, D.J. Salmon, S.T. Wilson and T.J. Meyer, Inorg. Chem., 18 (1979) 2472.
79 J. Leszczynski and W. Wojciechowski, J. Struct. Chem., 17 (1976) 168.
80 R.C. Dickinson, F.T. Helm, W.A. Baker, T.D. Black and W.H. Watson, Inorg. Chem. 16 (1977) 1530.
81 E. Grazynska and W. Wojciechowski, Pol. Akad. Nauk., Bull. Sci. Chim., 26 (1978) 393.
82 H. tom Dieck, Inorg. Chim. Acta, 7 (1973) 397.
83 L. Antolini, G. Marcotrigiano, L. Menabue and G.C. Pellacani, J. Am. Chem. Soc., 102 (1980) 5506.
84 P.J.M.W.L. Birker and H.C. Freeman, J. Am. Chem. Soc., 99 (1977) 6890.
85 D.B. Brown, J.R. Watson, J.W. Hall and W.E. Hatfield, Inorg. Chem., 16 (1977) 2526.
86 J.P. Fackler, Prog. Inorg. Chem., 21 (1976) 55.
87 H.J. Schugar, C.C. Ou, J.A. Thich, J.A. Potenza, T.R. Felthouse, M.S. Haddad, D.N. Hendrickson, W. Furey and R.A. Lalancette, Inorg. Chem., 19 (1980) 543.

88 D.B. Brown, J.A. Zubieta, P.A. Vella, J.T. Wrobleski, T. Watt, W.E. Hatfield and P. Day, Inorg. Chem., 19 (1980) 1945.
89 H.J. Mattausch, J.B. Hendricks, R. Eger, J.D. Corbett and A. Simon, Inorg. Chem., 19 (1980) 2128.
90 G.O. Evans, J.P. Hargaden and R.K. Sheline, J. Chem. Soc., Chem. Commun., (1967) 186.
91 E.H. Schubert and R.K. Sheline, Z. Naturforsch., Teil B, 20 (1965) 1306.
92 G.O. Evans and R.K. Sheline, J. Inorg. Nucl. Chem., 30 (1968) 2862.
93 R.J. Lawson and J.R. Shapley, J. Am. Chem. Soc., 98 (1976) 7433.
94 R.J. Lawson and J.R. Shapley, Inorg. Chem., 17 (1978) 772.
95 K. Wade, J. Chem. Soc. D, (1971) 792.
96 T.J. Katz and N. Acton, J. Am. Chem. Soc., 95 (1973) 2738.
97 M.D. Newton, J.M. Schulman and M.M. Manus, J. Am. Chem. Soc., 96 (1974) 17.
98 R.P. Brint, K. Pelin and T.R. Spalding, Inorg. Nucl. Chem. Lett., 16 (1980) 391.
99 D.M.P. Mingos, J. Chem. Soc., Dalton Trans., (1976) 1163.
100 M.S. Paquette and L.F. Dahl, J. Am. Chem. Soc., 102 (1980) 6621.
101 L. Pauling, Proc. Natl. Acad. Sci. U.S.A., 72 (1975) 3799.
102 L. Pauling, Proc. Natl. Acad. Sci. U.S.A., 72 (1975) 4200.
103 L. Pauling, Proc. Natl. Acad. Sci. U.S.A., 73 (1976) 274.
104 L. Pauling, Proc. Natl. Acad. Sci. U.S.A., 73 (1976) 4290.
105 L. Pauling, Proc. Natl. Acad. Sci. U.S.A., 74 (1977) 5235.
106 G.H. Duffey, J. Chem. Phys., 19 (1951) 963.
107 W.F. Libby, J. Chem. Phys., 46 (1967) 399.
108 E.M. Shustorovich and D.V. Korol'kov, J. Struct. Chem., 13 (1972) 634.
109 J.W. Lauher, J. Am. Chem. Soc., 100 (1978) 5305.
110 J.W. Lauher, J. Am. Chem. Soc., 101 (1979) 2604.
111 G. Ciani and A. Sironi, J. Organomet. Chem., 197 (1980) 233.
112 D.V. Korol'kov, J. Struct. Chem., 16 (1975) 749.
113 D.V. Korol'kov, J. Struct. Chem., 15 (1974) 902.
114 R.E. Benfield and B.F.G. Johnson, J. Chem. Soc., Dalton Trans., (1980) 1743.
115 J.D. Head and K.A.R. Mitchell, Mol. Phys., 35 (1978) 1681.
116 J.D. Head and K.A.R. Mitchell, Can. J. Chem., 57 (1979) 1826.
117 G. Blyholder, J. Chem. Phys., 62 (1975) 3193.
118 G. Blyholder, J. Vac. Sci. Technol., 11 (1974) 865.
119 D. Ajo, G. Granozzi, E. Tondello and I. Fragala, Inorg. Chim. Acta, 37 (1979) 191.
120 V.I. Baranovskii, O.V. Sizova and N.V. Ivanova, J. Struct. Chem., 17 (1976) 478.
121 R. Hoffmann, J. Chem. Phys., 39 (1968) 1397.
122 F.A. Cotton and T.E. Haas, Inorg. Chem., 3 (1964) 10.
123 M.R.V. Sahyun, J. Chem. Educ., 57 (1980) 239 and references therein.
124 R.P. Messmer, S.K. Knudson, K.H. Johnson, J.B. Diamond and C.Y. Yang, Phys. Rev. B, 13 (1976) 1396.
125 R.P. Messmer, Gazz. Chim. Ital., 109 (1980) 241.
126 R.P. Messmer, C.W. Tucker and K.H. Johnson, Chem. Phys. Lett., 36 (1975) 423.
127 J.P. Dahl and C.J. Ballhausen, Adv. Quant. Chem., 4 (1968) 170; M. Gerloch and R.C. Slade, Ligand-field Parameters, Cambridge University Press, Cambridge, 1973; C.J. Ballhausen, Molecular Electronic Structures of Transition Metal Complexes, McGraw-Hill, London, 1979.
128 C.J. Ballhausen, Ligand Field Theory, McGraw-Hill, New York, 1962; C.J. Ballhausen and H.B. Gray, Molecular Orbital Theory, W.A. Benjamin, Inc., New York, 1965.

129 M.B. Hall and R.F. Fenske, Inorg. Chem., 11 (1972) 768.
130 P. Hohenberg and W. Kohn, Phys. Rev. B, 136 (1964) 864.
131 J.C. Slater, The Self-consistent Field for Molecules and Solids, McGraw-Hill, New York, 1974.
132 M. Benard and A. Viellard, Nouv. J. Chim., 1 (1977) 97.
133 K.H. Johnson, Annu. Rev. Phys. Chem., 26 (1975) 39.
134 D.E. Ellis and G.H. Painter, Phys. Rev. B, 2 (1970) 2887.
135 E.J. Baerends, D.E. Ellis and P. Ros, Chem. Phys., 2 (1973) 41.
136 D.E. Ellis, A. Rosen, H. Adachi and F.W. Averill, J. Chem. Phys., 65 (1976) 3629.
137 R.C. Baetzold, J. Catal., 29 (1973) 129.
138 R.C. Baetzold, Comments Solid State Phys., 4 (1972) 62.
139 E.L. Muetterties, Chem. Rev., 79 (1979) 91 and references therein.
140 A.B. Anderson, J. Chem. Phys., 68 (1979) 1744.
141 A.B. Anderson, Proc. Int. Conf. Phys. Transition Met., (1977) 379.
142 D.W. Bullett and E.P. O'Reilly, Surf. Sci., 89 (1979) 274.
143 R.C. Baetzold, Surf. Sci., 36 (1972) 123.
144 N. Rösch and D. Menzel, Chem. Phys., 13 (1976) 243.
145 A.B. Anderson, J. Chem. Phys., 64 (1976) 4046.
146 E. Shustorovich and R.C. Baetzold, J. Am. Chem. Soc., 102 (1980) 5989.
147 E.L. Muetterties, Angew. Chem. Int. Ed. Engl., 17 (1978) 545.
148 G. Blyholder and C.A. Coulson, Trans. Faraday Soc., 63 (1967) 1782.
149 J. Koutecky, Adv. Chem. Phys., 9 (1965) 85.
150 L.W. Anders, R.S. Hansen and L.S. Bartell, J. Chem. Phys., 62 (1975) 1641.
151 L.W. Anders, R.S. Hansen and L.S. Bartell, J. Chem. Phys., 59 (1973) 5277.
152 A.B. Anderson and R. Hoffmann, J. Chem. Phys., 61 (1974) 4545.
153 J.P. Van Dyke, J. Nucl. Mater., 69–70 (1978) 583.
154 B.J. Thorpe, Surf. Sci., 33 (1972) 306.
155 T.P. Grimsley and B.J. Thorpe, J. Phys., F1 (1971) L4.
156 T.B. Grimsley and B.J. Thorpe, Phys. Lett. A, 37 (1971) 459.
157 T.B. Grimsley, Adv. Catal., 12 (1960) 1.
158 G.A. Ozin, Coord. Chem. Rev., 28 (1979) 117.
159 G. Doyen and G. Ertl, Surf. Sci., 43 (1974) 197.
160 A.B. Anderson, J. Chem. Phys., 66 (1977) 5108.
161 H. Basch, M.D. Newton and J.W. Moskowitz, J. Chem. Phys., 73 (1980) 4492.
162 (a) R.C. Baetzold, J. Chem. Phys., 55 (1971) 4363.
(b) R.C. Baetzold and R.E. Mack, J. Chem. Phys., 62 (1975) 1513.
163 C.Y. Yang and G. Bambakzdis, Proc. Int. Conf. Physics. Transition Met., (1977) 363.
164 C.F. Melius, T.H. Upton and W.A. Goddard, Solid State Commun., 28 (1978) 501.
165 A. Kawataba, J. Phys. Soc. Jpn., 29 (1970) 902.
166 T. Welker and T.P. Martin, J. Chem. Phys., 70 (1979) 5683.
167 (a) W. Schulze, H.U. Becker and H. Abe, Ber. Bunsenges. Phys. Chem., 82 (1978) 138.
(b) W. Schulze, H.U. Becker and H. Abe, Chem. Phys., 35 (1978) 177.
168 G.A. Ozin and W.E. Klotzbücher, Inorg. Chem., 18 (1979) 2101.
169 F. Forstmann, D.M. Kolb, D. Leutloff and W. Schulze, J. Chem. Phys., 66 (1977) 2806.
170 F. Forstmann and D.M. Kolb, Ber. Bunsenges. Phys. Chem., 82 (1978) 30.
171 Ji-Qing Xu, Chi-Lin Ta Hsueh, Tzu Jan K'o Hsueh Hsueh Pa, (1980) 83.
172 P.W. Anderson, Phys. Rev., 124 (1961) 41.
173 J. Hubbard, Proc. R. Soc. Ser. A, 276 (1963) 238.
174 J. Hubbard, Proc. R. Soc. Ser. A, 277 (1964) 237.

175 R.P. Messmer, D.R. Salahub, K.H. Johnson and C.Y. Yang, Chem. Phys. Lett., 51 (1977) 84.
176 D.J.M. Fassaert, H. Verbeek and A. Van der Avoird, Surf. Sci., 29 (1972) 501.
177 G. Blyholder, J. Chem. Soc., Chem. Commun., (1973) 625.
178 D.M. Newns, Phys. Rev., 178 (1969) 1123.
179 M. Watanabe, Surf. Sci., 34 (1973) 759.
180 G.C. Bond, Catalysis by Metals, Academic Press, New York, 1962.
181 D. Shopov, A. Andreev and D. Petrov, J. Catal., 13 (1969) 123.
182 P. Jena, F.Y. Fradin and D.E. Ellis, Phys. Rev. B, 3 (1979) 3543.
183 J.C. Robertson and C.W. Wilmsen, J. Vac. Sci. Technol., 9 (1972) 901.
184 R.L. Park and H.E. Farnsworth, J. Chem. Phys., 43 (1965) 2351.
185 N. Rösch, in P. Phariseau and L. Schiere (Eds.), Electrons in Finite and Infinite Structures, Vol. 24, NATO Adv. Study Inst. Ser., Plenum Press, 1977, p. 1.
186 D.E. Ellis, E.J. Baerends, H. Adachi and F.W. Averill, Surf. Sci., 64 (1977) 649.
187 A. Rosen, E.J. Baerends and D.E. Ellis, Surf. Sci., 82 (1979) 139.
188 I.P. Batra and O. Robaux, J. Vac. Sci. Technol., 12 (1975) 242.
189 I.P. Batra and P.S. Bagus, Solid State Commun., 16 (1975) 1097.
190 A.A. Ballman, J.R. Carruthers and H.M. O'Bryan, J. Cryst. Growth, 6 (1970) 184.
191 J.C. Toledano, Ann. Telecommun., 29 (1974) 249.
192 J. Dunken, H.G. Fritsche, P. Kadura, L.D. Künne, H. Müller and G. Opitz, Z. Chem., 12 (1972) 433.
193 K.H. Johnson, in R. Vanselow (Ed.), Chemistry and Physics of Solid Surfaces, Vol. 2, CRC Press, 1979, p. 21 and references therein.
194 G.A. Ozin, Faraday Symp. Chem. Soc., 14 (1980) 1.
195 (a) G. Seifert, E. Mrosan and H. Müller, Phys. Status Solidii B, 89 (1978) 553.
(b) G. Seifert, E. Mrosan, H. Müller and P. Ziesche, Phys. Status Solidii B, 89 (1978) K175.
196 J.D. Head, K.A.R. Mitchell and L. Noodleman, Surf. Sci., 69 (1977) 714.
197 I.P. Batra and O. Robaux, Surf. Sci., 49 (1975) 653.
198 B.D. El-Issa and A. Hinchliffe, Mol. Phys., 39 (1980) 1463.
199 T.B. Grimsley, J. Vac. Sci. Technol., 8 (1971) 31.
200 J.P. Gaspard, Proc. Int. Conf. Physics Transition Met., (1977) 360.
201 D.V. Korol'kov and V.N. Pak, Teor. Eksp. Khim., 7 (1971) 531.
202 D.V. Korol'kov, K. Miessner and K.V. Ovchinnikov, J. Struct. Chem., 14 (1974) 661.
203 D.V. Korol'kov and H. Miessner, Vestn. Leningrad. Univ., Fiz. Khim., (1974) 82.
204 F.A. Cotton and G.G. Stanley, Chem. Phys. Lett., 58 (1978) 450.
205 W.C. Trogler, D.E. Ellis and J. Berkowitz, J. Am. Chem. Soc., 101 (1979) 5896.
206 B.E. Bursten, F.A. Cotton, J.C. Green, E.A. Seddon and G.G. Stanley, J. Am. Chem. Soc., 102 (1980) 955.
207 D.A. Brown, J. Inorg. Nucl. Chem., 5 (1958) 289.
208 R.K. Sheline, J. Am. Chem. Soc., 73 (1951) 1615.
209 F.A. Cotton and J.M. Troup, J. Am. Chem. Soc., 96 (1974) 4155.
210 C.H. Wei and L.F. Dahl, J. Am. Chem. Soc., 91 (1969) 1351.
211 D.V. Korol'kov and H. Miessner, Z. Phys. Chem. (Leipzig), 253 (1973) 25.
212 I.A. Oxton, Inorg. Chem., 19 (1980) 2825.
213 D.R. Tyler, R.A. Levenson and H.B. Gray, J. Am. Chem. Soc., 100 (1978) 7888.
214 B. Delley, M.C. Manning, D.E. Ellis, J. Berkowitz and W.C. Trogler, submitted for publication.
215 B.E.R. Schilling and R. Hoffmann, J. Am. Chem. Soc., 101 (1979) 3456.

216 M. Elian, M.M.L. Chen, D.M.P. Mingos and R. Hoffmann, Inorg. Chem., 15 (1976) 1148.
217 M. Elian and R. Hoffmann, Inorg. Chem., 14 (1975) 1058.
218 J.W. Lauher, M. Elian, R.H. Summerville and R. Hoffmann, J. Am. Chem. Soc., 98 (1976) 3219.
219 T.A. Albright, R. Hoffmann, J.C. Thibault and D.L. Thorn, J. Am. Chem. Soc., 101 (1979) 3801.
220 A. Dedieu and R. Hoffmann, J. Am. Chem. Soc., 100 (1978) 2074.
221 A.S. Foust, M.S. Foster and L.F. Dahl, J. Am. Chem. Soc., 91 (1969) 5633 and references therein.
222 J. Halpern, Adv. Chem. Ser., 70 (1968) 1.
223 J. Evans, J. Chem. Soc., Dalton Trans., (1980) 1005.
224 D.L. Stevenson, C.H. Wei and L.F. Dahl, J. Am. Chem. Soc., 93 (1971) 6027.
225 C.E. Strouse and L.F. Dahl, Discuss. Faraday Soc., 47 (1969) 93.
226 C.E. Strouse and L.F. Dahl, J. Am. Chem. Soc., 93 (1971) 6032.
227 C.H. Wei and L.F. Dahl, J. Am. Chem. Soc., 90 (1968) 3960.
228 C.A. Coulson, Proc. R. Soc. Ser. A, 169 (1938) 413.
229 H. Vahrenkamp, V.A. Uchtman and L.F. Dahl, J. Am. Chem. Soc., 90 (1968) 3272.
230 D.W. Bullett, Inorg. Chem., 19 (1980) 1780.
231 F.A. Cotton, Inorg. Chem., 3 (1964) 1217.
232 S.J. Cartwright, K.R. Dixon and A.D. Rattray, Inorg. Chem., 19 (1980) 1120.
233 A.R. Pinhas, T.A. Albright, P. Hoffman and R. Hoffmann, Helv. Chim. Acta, 63 (1980) 29.
234 Trinh-Toan, W.P. Fehlhammer and L.F. Dahl, J. Am. Chem. Soc., 94 (1972) 3389.
235 Trinh-Toan, B.K. Teo, J.A. Ferguson, T.J. Meyer and L.F. Dahl, J. Am. Chem. Soc., 99 (1977) 408.
236 R.S. Gall, C.T.W. Chu and L.F. Dahl, J. Am. Chem. Soc., 96 (1974) 4019.
237 C.Y. Yang, K.H. Johnson, R.H. Holm and J.G. Norman, J. Am. Chem. Soc., 97 (1975) 6596.
238 D.V. Korol'kov and H. Miessner, Vestn. Leningrad. Univ., Fiz. Khim., (1974) 82.
239 H.J. Freund and G. Hohlneicher, Theor. Chim. Acta, 51 (1979) 145.
240 R. Hoffmann, B.A.R. Schilling, R. Bau, H.D. Kaesz and D.M.P. Mingos, J. Am. Chem. Soc., 100 (1978) 6088.
241 G. Huttner and H. Lorenz, Chem. Ber., 107 (1974) 996.
242 T.F. Koetzle, R.K. McMullan, R. Bau, D.W. Hart, R.G. Teller, D.L. Lipton and R.D. Wilson, Adv. Chem. Ser., 167 (1978) 61.
243 J. Müller, H. Dorner, G. Huttner and H. Lorenz, Angew. Chem. Int. Ed. Engl., 12 (1973) 1005.
244 R.G. Vranka, L.F. Dahl, P. Chini and J. Chatt, J. Am. Chem. Soc., 91 (1969) 1574.
245 M.J. Bennett, F.A. Cotton and B.H.C. Winquist, J. Am. Chem. Soc., 89 (1967) 5366.
246 O. Pivesna and P.F. Zanazzi, Angew. Chem. Int. Ed. Engl., 19 (1980) 561.
247 A. Dedieu and R. Hoffmann, J. Am. Chem. Soc., 100 (1978) 2074.
248 K.R. Mann, J.G. Gordon and H.B. Gray, J. Am. Chem. Soc., 97 (1975) 3553.
249 N.S. Lewis, K.R. Mann, J.G. Gordon and H.B. Gray, J. Am. Chem. Soc., 98 (1976) 7461.
250 K.R. Mann, N.S. Lewis, R.M. Williams, H.B. Gray and J.G. Gordon, Inorg. Chem., 17 (1978) 828.
251 V.M. Miskowski, G.L. Nobinger, D.S. Kliger, G.S. Hammond, N.S. Lewis, K.R. Mann and H.B. Gray, J. Am. Chem. Soc., 100 (1978) 485.
252 S. Stensvad, B.J. Helland, M.W. Babich, R.A. Jacobson and R.E. McCarley, J. Am. Chem. Soc., 100 (1978) 6257.

253 J.K. Ruff, R.P. White and L.F. Dahl, J. Am. Chem. Soc., 93 (1971) 2159.
254 H. Vahrenkamp and L.F. Dahl, Angew. Chem. Int. Ed. Engl., 8 (1969) 144.
255 L.D. Crossman, D.P. Olsen and G.H. Duffey, J. Chem. Phys., 38 (1963) 73.
256 D.V. Korol'kov and V.N. Pak, J. Struct. Chem., 14 (1973) 1027.
257 D.V. Korol'kov and V.N. Pak, J. Struct. Chem., 12 (1971) 282.
258 L.J. Guggenberger and A.W. Sleight, Inorg. Chem., 8 (1969) 2041.
259 G. Seifert, J. Finster and H. Müller, Chem. Phys. Lett., 75 (1980) 373.
260 P.A. Vaughn, J.H. Sturdivant and L. Pauling, J. Am. Chem. Soc., 72 (1950) 5477.
261 N.S. Voronovich and D.V. Korol'kov, J. Struct. Chem., 12 (1971) 458.
262 N.S. Voronovich and D.V. Korol'kov, J. Struct. Chem., 12 (1971) 613.
263 H. Müller, Z. Phys. Chem. (Liepzig), 249 (1972) 1.
264 P.A. Edwards, R.E. McCarley and D.R. Torgeson, Inorg. Chem., 11 (1972) 1185.
265 J. Wirsich, Theor. Chim. Acta, 34 (1974) 67.
266 D.M.P. Mingos, J. Chem. Soc., Dalton Trans., (1974) 133.
267 D.M.P. Mingos and M.I. Forsyth, J. Chem. Soc., Dalton Trans., (1977) 610.
268 R.G. Wooley, Chem. Phys. Lett., 71 (1980) 135.
269 K.H. Chang and R.G. Wooley, J. Phys. C, 12 (1979) 2745.
270 C.H. Wei and L.F. Dahl, J. Am. Chem. Soc., 90 (1968) 3977.
271 D.M.P. Mingos, J. Chem. Soc., Dalton Trans., (1976) 1163.
272 P.L. Bellon, M. Manaserro, L. Naldini and M. Sansoni, J. Chem. Soc., Chem. Commun., (1972) 1035.
273 P.L. Bellon, M. Manaserro and M. Sansoni, J. Chem. Soc., Dalton Trans., (1973) 2423.
274 M. McPartlin, R. Mason and L. Malatesta, J. Chem. Soc., Chem. Commun., (1969) 334.
275 H. Basch and H.B. Gray, Theor. Chim. Acta, 4 (1966) 367.
276 E. Clementi, J. Chem. Phys., 40 (1964) 1944.
277 E.W. Plummer, W.R. Salaneck and J.S. Miller, Phys. Rev. B, 18 (1978) 1673.
278 R.A. Walton, Prog. Inorg. Chem., 21 (1976) 105.
279 S.C. Avanzino and W.L. Jolly, J. Am. Chem. Soc., 98 (1976) 6505.
280 F.P. Netzer, E. Bertel and J.A.D. Matthews, J. Electron Spectrosc. Relat. Phenom., 18 (1980) 199.
281 G. Apai, S.T. Lee, M.G. Mason, L.J. Gerenser and S.A. Garner, J. Am. Chem. Soc., 101 (1979) 6880.
282 M.J. Jun and F.J. Müller, Monatsh. Chem., 103 (1972) 1213.
283 K. Farmery, M. Kilner, R. Greatrex and N.N. Greenwood, J. Chem. Soc. A, (1969) 2339.
284 L.F. Dahl and J.F. Blount, Inorg. Chem., 4 (1965) 1373.
285 D.G. Tisley and R.A. Walton, J. Inorg. Nucl. Chem., 35 (1973) 1905.
286 D.G. Tisley and R.A. Walton, Inorg. Chem., 12 (1973) 373.
287 A.D. Hamer and R.A. Walton, Inorg. Chem., 13 (1974) 1446.
288 J. Finster, P. Muller and A. Meisel, Proc. 18th Int. Colloq. Spec., (1975) 596.
289 C. Battistoni, G. Mattogno, F. Cariati, L. Naldini and A. Sgamelloti, Inorg. Chim. Acta, 24 (1977) 207.
290 P.M.Th.M. van Attekum, J.W.A. van der Velden and J.M. Trooster, Inorg. Chem., 19 (1980) 701.
291 T. Herskovitz, B.A. Averill, R.H. Holm, J.A. Ibers, W.D. Philipps and J.F. Weiher, Proc. Natl. Acad. Sci. U.S.A., 69 (1972) 2437.
292 A. Müller, R. Jostes, W. Jaegermann and R.G. Bhattacharyya, Inorg. Chim. Acta, 41 (1980) 259.
293 J.C. Green, E.A. Seddon and D.M.P. Mingos, J. Chem. Soc., Chem. Commun., (1979) 94.
294 J.C. Green, D.M.P. Mingos and E.A. Seddon, J. Organomet. Chem., 185 (1980) C20.

295 H. Conrad, G. Ertl, H. Knözinger, J. Küppers and E.E. Latta, Chem. Phys. Lett., 42 (1976) 115.
296 G. Herzberg, Electronic Spectra of Polyatomic Molecules, Van Nostrand–Reinhold, New York, 1966.
297 W.J. Power and G.A. Ozin, Adv. Inorg. Chem. Radiochem., 23 (1980) 79.
298 G.A. Ozin and H. Huber, Inorg. Chem., 17 (1978) 155.
299 G.A. Ozin, H. Huber and S.A. Mitchell, Inorg. Chem., 18 (1979) 2932.
300 S.A. Mitchell and G.A. Ozin, J. Am. Chem. Soc., 100 (1978) 6776.
301 W.E. Klotzbücher and G.A. Ozin, J. Am. Chem. Soc., 100 (1978) 2262.
302 G.A. Ozin and W.E. Klotzbücher, J. Mol. Catal., 3 (1977) 195.
303 M. Moskovits and J.E. Hulse, Proc. Int. Conf. Physics Transition Met., (1977) 368.
304 M. Moskovits and J.E. Hulse, J. Chem. Soc., Faraday Trans. 2, (1977) 471.
305 (a) M. Moskovits and J.E. Hulse, J. Chem. Phys., 66 (1977) 3988.
(b) W.E. Klotzbücher and G.A. Ozin, Inorg. Chem., 19 (1980) 3767.
306 M. Moskovits and J.E. Hulse, J. Chem. Phys., 67 (1977) 4271.
307 (a) G.A. Ozin and C.G. Francis, J. Mol. Struct., 59 (1980) 55.
(b) C.G. Francis, H. Huber and G.A. Ozin, Inorg. Chem., 19 (1980) 219.
308 A.J.L. Hanlan and G.A. Ozin, Inorg. Chem., 16 (1977) 2857.
309 B.H. Robinson and J.E. Ferguson, J. Chem. Soc., (1964) 5683.
310 F.A. Cotton and J.T. Mague, Inorg. Chem., 3 (1964) 1094.
311 F.A. Cotton and J.T. Mague, Inorg. Chem., 3 (1964) 1402.
312 F.A. Cotton and S.J. Lippard, J. Am. Chem. Soc., 86 (1964) 4497.
313 F.A. Cotton, S.J. Lippard and J.T. Mague, Inorg. Chem., 4 (1965) 508.
314 R.A. Bailey and J.A. McIntyre, Inorg. Chem., 5 (1966) 1940.
315 F.A. Cotton and S.J. Lippard, Inorg. Chem., 4 (1965) 59.
316 J.C. Sheldon, Nature (London), 184 (1959) 1210.
317 J.C. Sheldon, J. Chem. Soc., (1960) 1007.
318 R.F. Schneider and R.A. Mackay, J. Chem. Phys., 48 (1968) 843.
319 R.C. Allen and J.C. Sheldon, Aust. J. Chem., 18 (1965) 277.
320 P.B. Fleming, L.A. Muller and R.E. McCarley, Inorg. Chem., 6 (1967) 1.
321 D.J. Robbins and A.J. Thomson, J. Chem. Soc., Dalton Trans., (1972) 2350.
322 J.H. Espenson and R.E. McCarley, J. Am. Chem. Soc., 88 (1966) 1063.
323 A. Broll, A. Simon, H.G. von Schnering and H. Schäfer, Z. Anorg. Allg. Chem., 367 (1969) 1.
324 R.A. Mackay and R.F. Schneider, Inorg. Chem., 6 (1967) 549.
325 J.G. Converse and R.E. McCarley, Inorg. Chem., 9 (1970) 1361.
326 R.B. King, D.M. Braitsch and P.N. Kapoor, J. Am. Chem. Soc., 97 (1975) 60.
327 J.A. Ferguson and T.J. Meyer, J. Am. Chem. Soc., 94 (1972) 3409.
328 C.R. Bock and M.S. Wrighton, Inorg. Chem., 16 (1977) 1309.
329 E.M. Kosower, J. Am. Chem. Soc., 80 (1958) 3253.
330 E.M. Kosower, J. Am. Chem. Soc., 80 (1958) 3261.
331 M.J. Jun and F.J. Müller, Monatsh. Chem., 103 (1972) 1213.
332 W. Hieber and H. Beutner, Z. Naturforsch., Teil B, 17 (1962) 211.
333 D.B.W. Yawney and F.G.A. Stone, J. Chem. Soc. A, (1969) 502.
334 P. Chini, Pure Appl. Chem., 23 (1970) 489.
335 S. Martinengo, P. Chini, V.G. Albano, F. Cariati and T. Salvatori, J. Organomet. Chem., 59 (1973) 379.
336 P.C. Steinhardt, W.L. Gladfelter, A.D. Harley, J.R. Fox and G.L. Geoffroy, Inorg. Chem., 19 (1980) 332.

337 G.L. Geoffroy and W.L. Gladfelter, J. Am. Chem. Soc., 99 (1977) 304.
338 R.A. Epstein, T.R. Gaffney, G.L. Geoffroy, W.L. Gladfelter and R.S. Henderson, J. Am. Chem. Soc., 101 (1979) 3847.
339 K. Dus, H. De Klerk, K. Sletten and R.G. Bartsch, Biochim. Biophys. Acta, 140 (1967) 291.
340 J.S. Hong and J.C. Rabinowitz, J. Biol. Chem., 245 (1970) 4982.
341 D. Coucouvanis, E.D. Simhon and N.C. Baenziger, J. Am. Chem. Soc., 102 (1980) 6644.
342 G.O. Morpugo, V. Mosini, P. Porta, G. Dessy and V. Fares, J. Chem. Soc., Dalton Trans., (1980) 1272.
343 S.Otsuka, A. Nakamura and T. Yoshida, Inorg. Chem., 7 (1968) 261.
344 H. Wong, D. Sedney, W.M. Reiff, R.B. Frankel, T.J. Meyer and D. Salmon, Inorg. Chem., 17 (1978) 194.
345 R.J. Elliot, Phys. Rev., 96 (1954) 266.
346 G.A. Ozin, J. Am. Chem. Soc., 102 (1980) 3301.
347 G.W. Eastland, M.A. Mazid, D.R. Russell and M.C.R. Symons, J. Chem. Soc., Dalton Trans., (1980) 1682.
348 Y. Kim and K. Seff, J. Am. Chem. Soc., 99 (1977) 7055.
349 Y. Kim and K. Seff, J. Am. Chem. Soc., 100 (1978) 175.
350 N.C. Baenziger and A.W. Struss, Inorg. Chem., 15 (1976) 1807.
351 G.W. Hunt, T.C. Lee and E.L. Amma, J. Inorg. Nucl. Chem. Lett., 10 (1974) 909.
352 B.K. Teo and J.C. Calabrese, J. Am. Chem. Soc., 97 (1975) 1256.
353 S.M. Nelson, S.G. McFall, M.G.B. Drew and A.H. bin Othman, J. Chem. Soc., Chem. Commun., (1977) 370.
354 S.Z. Goldberg, B. Savack, G. Stanley, R. Eisenberg, D.M. Braitsch, J.S. Miller and M. Abkowitz, J. Am. Chem. Soc., 99 (1977) 110.
355 J.F. Gibson and P.O. Meier, J. Chem. Res., (1978) 66.
356 B.M. Peake, B.H. Robinson, J. Simpson and D.J. Watson, Inorg. Chem., 16 (1977) 405.
357 H.C. Longuet-Higgins and A.J. Stone, Mol. Phys., 5 (1962) 417.
358 B.M. Peake, B.H. Robinson, J. Simpson and D.J. Watson, J. Chem. Soc., Chem. Commun., (1974) 945.
359 D. Miholva, J. Klima and A.A. Vlcek, Inorg. Chim. Acta, 27 (1978) L67.
360 A.M. Bond, P.A. Dawson, B.M. Peake, B.H. Robinson and J. Simpson, Inorg. Chem., 16 (1977) 2199.
361 H.C. Silvis, R.H. Tieckelmann and B.A. Averill, Inorg. Chim. Acta, 36 (1979) L423.
362 J.W. McDonald, G.D. Friesen and W.E. Newton, Inorg. Chim. Acta, 46 (1980) L79.
363 R.B. King, Inorg. Chem., 5 (1966) 2227.
364 J.E. Ferguson and T.J. Meyer, J. Am. Chem. Soc., 94 (1972) 3409.
365 M. Poe, W.D. Philips, C.C. McDonald and W.H. Orme-Johnson, Biochem. Biophys. Res. Commun., 42 (1971) 705.
366 R.E. Dessy, R.B. King and M. Waldrop, J. Am. Chem. Soc., 88 (1966) 5112.
367 D.L. Rousseau, J.M. Friedman and P.F. Williams, Topics Curr. Phys., 11 (1978) 203.
368 T.G. Spiro and P. Stein, Annu. Rev. Phys. Chem., 28 (1977) 501.
369 A.C. Albrecht and M.C. Hutley, J. Chem. Phys., 55 (1971) 4438.
370 A.C. Albrecht, J. Chem. Phys., 34 (1961) 1476.
371 M.Z. Zgierski and M. Pawlikowski, J. Chem. Phys., 71 (1979) 2025.
372 W.F. Howard and L. Andrews, Inorg. Chem., 14 (1975) 1726.
373 C. Cousrisseau, J. Raman Spectrosc., 6 (1977) 303.
374 S. Onaka and D.F. Shriver, Inorg. Chem., 15 (1976) 915.
375 R.G. Austin, R.S. Paonessa, P.J. Giordano and M.S. Wrighton, Adv. Chem. Ser., 168 (1978) 189.

376 E.W. Burkhardt and G.L. Geoffroy, J. Organomet. Chem., 198 (1980) 179.
377 (a) A. Terzis and T.G. Sprio, J. Chem. Soc., Chem. Commun., (1970) 1160.
(b) M. Moskovits and D.P. DiLella, J. Chem. Phys., 72 (1980) 2267.
378 R. Greatrex and N.N. Greenwood, Discuss. Faraday Soc., 47 (1969) 126.
379 T.H. Moss, A.J. Bearden, R.G. Bartsch, M.A. Cusanovich and A. San Pietro, Biochemistry, 7 (1968) 1591.
380 M.C.W. Evans, D.O. Hall and C.E. Johnson, Biochem. J., 119 (1970) 289.
381 D.C. Blomstrom, E. Knight, W.D. Philips and J.F. Weiher, Proc. Natl. Acad. Sci. U.S.A., 51 (1964) 1085.
382 J. Knight and M.J. Mays, J. Chem. Soc. A, (1970) 654.
383 C.G. Cooke and M.J. Mays, J. Chem. Soc., Dalton Trans., (1975) 455.
384 F.A. Vollenbroek, P.C.P. Trouten, J.M. Trooster, J.P. Van den Berg and J.J. Bour, Inorg. Chem., 17 (1978) 1345.
385 S.A.R. Knox and F.G.A. Stone, J. Chem. Soc. A, (1969) 2559.
386 S.A.R. Knox and F.G.A. Stone, J. Chem. Soc. A, (1970) 3147.
387 S.A.R. Knox and F.G.A. Stone, J. Chem. Soc. A, (1971) 2874.
388 A. Brookes, S.A.R. Knox and F.G.A. Stone, J. Chem. Soc. A, (1971) 3469.
389 B.F.G. Johnson, J. Lewis and M.V. Twigg, J. Organomet. Chem., 67 (1974) C75.
390 F.A. Cotton, A.J. Deeming, P.L. Josty, S.S. Ullah, A.J.P. Domingos, B.F.G. Johnson and J. Lewis, J. Am. Chem. Soc., 93 (1971) 4624.
391 D.R. Tyler, M. Altobelli and H.B. Gray, J. Am. Chem. Soc., 102 (1980) 3022.
392 W.R. Cullen, D.A. Harbourne, B.V. Liengme and J.R. Sams, J. Am. Chem. Soc., 90 (1968) 3293.
393 W.R. Cullen, D.A. Harbourne, B.V. Liengme and J.R. Sams, Inorg. Chem., 9 (1970) 702.
394 W.R. Cullen and D.A. Harbourne, Inorg. Chem., 9 (1970) 1839.
395 P.J. Roberts and J. Trotter, J. Chem. Soc. A, (1971) 1479.
396 J.L. Graff, R.O. Sanner and M.S. Wrighton, J. Am. Chem. Soc., 101 (1979) 273.
397 F. Asinger, B. Fell and K. Schrage, Chem. Ber., 98 (1964) 372.
398 M.D. Carr, V.V. Kane and M.C. Whiting, Proc. Chem. Soc., (1964) 408.
399 J.L. Graff, R.D. Sanner and M.S. Wrighton, Gov. Rep. Announce. (U.S.), 79 (1979) 91.
400 J.L. Graff and M.S. Wrighton, J. Am. Chem. Soc., 102 (1980) 2123.
401 B.F.G. Johnson, J.W. Kelland, J. Lewis and S.K. Rehani, J. Organomet. Chem., 113 (1976) C42.
402 S. Bhaduri, B.F.G. Johnson, J.W. Kelland, J. Lewis, P.R. Raithby, S. Rehani, G.M. Sheldrick, K. Wong and M. McPartlin, J. Chem. Soc., Dalton Trans., (1979) 562.
403 G.L. Geoffroy, Prog. Inorg. Chem., 27 (1980) 123.
404 G.L. Geoffroy and R.A. Epstein, Inorg. Chem., 16 (1977) 2795.
405 P.F. Heveldt, B.F.G. Johnson, J. Lewis, P.R. Raithby and G.M. Sheldrick, J. Chem. Soc., Chem. Commun., (1978) 340.
406 I.S. Sigal, K.R. Mann and H.B. Gray. J. Am. Chem. Soc., 102 (1980) 7252.